Antigen presentation safeguards the integrity of the hematopoietic stem cell pool

Hernández-Malmierca P., Vonficht D., Schnell A., Uckelmann H.J., Bollhagen A., Mahmoud M.A.A., Landua S.L., van der Salm E., Trautmann C., Raffel S., Grünschläger F., Lutz R., Ghosh M., Renders S., Correia N., Donato E., Dixon K.O., Hirche C., Andresen C., Robens Cl., Werner P.S., Boch T., Eisel D., Osen W., Pilz F., Przybylla A., Klein C., Buchholz F., Milsom M.D., Essers M.A.G., Eichmüller S.B., Hofmann W.K., Nowak D., Hübschmann D., Hundemer M., Thiede C., Bullinger L., Müller-Tidow C., Armstrong S.A., Trumpp A., Kuchroo V.K., Haas S.

This is the final version of the accepted manuscript. The original article has been published in final edited form in:

Cell Stem Cell
2022 MAY 05 ; 29(5): 760-775
doi: 10.1016/j.stem.2022.04.007

Publisher: Cell Press / Elsevier

Antigen presentation safeguards the integrity of the hematopoietic stem cell pool

Hernández-Malmierca P[1,2,3,#], Vonficht D[1,2,3,#], Schnell A[4,5,#], Uckelmann HJ[6,7], Bollhagen A[1,2], Mahmoud MAA[1,2], Landua SL[1,2], Van der Salm E[1,2], Trautmann CL[1,2], Raffel S[8,] Grünschläger F[1,2,3], Lutz R[1,2,8], Ghosh M[9], Renders S[1,2,8], Correia NC[1,2], Donato E[1,2], Dixon KO[4,5], Hirche C[1,10], Andresen C[1,2,3], Robens C[1,2], Werner PS[1,10], Boch T[1,2,11,12], Eisel D[13], Osen W[13], Pilz F[1,10], Przybylla A[1,2], Klein C[1,2], Buchholz F[14], Milsom MD[1,15], Essers MAG[1,10], Eichmüller SB[13], Hofmann WK[11,12], Nowak D[11,12], Hübschmann D[1,16,17], Hundemer M[8], Thiede C[14,17], Bullinger L[17,18], Müller-Tidow C[8], Armstrong SA[6,7], Trumpp A[1,2,17,*], Kuchroo VK[4,5,*], Haas S[1,2,17,18,19,20*]

[1] Heidelberg Institute for Stem Cell Technology and Experimental Medicine (HI-STEM gGmbH), 69120 Heidelberg, Germany.
[2] Division of Stem Cells and Cancer, Deutsches Krebsforschungszentrum (DKFZ) and DKFZ-ZMBH Alliance, 69120 Heidelberg, Germany.
[3] Faculty of Biosciences, Heidelberg University, 69117 Heidelberg, Germany
[4] Evergrande Center for Immunologic Diseases, Harvard Medical School and Brigham and Women's Hospital, Boston, MA 02115, USA.
[5] Klarman Cell Observatory, Broad Institute of MIT and Harvard, Cambridge, MA 02142, USA
[6] Department of Pediatric Oncology, Dana-Farber Cancer Institute, and Division of Hematology/Oncology, Boston, MA, USA.
[7] Boston Children's Hospital and Harvard Medical School, Boston, MA, USA.
[8] Department of Hematology, Oncology and Rheumatology, University of Heidelberg, 69120 Heidelberg, Germany.
[9] Department of Immunology, Institute for Cell Biology, University of Tübingen, Tübingen, Germany.
[10] Division of Inflammatory Stress in Stem Cells, Deutsches Krebsforschungszentrum (DKFZ) and DKFZ-ZMBH Alliance, 69120 Heidelberg, Germany.
[11] Department of Hematology and Oncology, University Hospital Mannheim, Mannheim, Germany.
[12] Medical Faculty Mannheim, Heidelberg University, Mannheim, Germany.
[13] Research Group GMP & T Cell Therapy, Deutsches Krebsforschungszentrum (DKFZ), 69120 Heidelberg, Germany.
[14] Faculty of Medicine, TU and University Hospital Dresden, Dresden, Germany.
[15] Division of Experimental Hematology, Deutsches Krebsforschungszentrum (DKFZ) and DKFZ-ZMBH Alliance, 69120 Heidelberg, Germany.
[16] Computational Oncology, Molecular Diagnostics Program, National Center for Tumor Diseases (NCT) Heidelberg and Deutsches Krebsforschungszentrum (DKFZ), Heidelberg, Germany
[17] German Cancer Consortium (DKTK), 69120 Heidelberg, Germany.
[18] Department of Hematology, Oncology and Tumor Immunology, Charité University Medicine, Berlin, Germany.
[19] Berlin Institute of Health (BIH) at Charité – Universitätsmedizin Berlin, 10117 Berlin, Germany
[20] Berlin Institute for Medical Systems Biology, Max Delbrück Center for Molecular Medicine in the Helmholtz Association, 10115 Berlin, Germany
[#] These authors contributed equally to this work
[*]Correspondence: a.trumpp@Dkfz-Heidelberg.de, vkuchroo@evergrande.hms.harvard.edu and simon.haas@bih-charite.de

Summary

Hematopoietic stem and progenitor cells (HSPCs) are responsible for the production of blood and immune cells. Throughout life, HSPCs acquire oncogenic aberrations that can cause hematological cancers. While molecular programs maintaining stem cell integrity have been identified, safety mechanisms eliminating malignant HSPCs from the stem cell pool remain poorly characterized. Here we show that HSPCs constitutively present antigens via major histocompatibility complex class II. The presentation of immunogenic antigens, as occurring during malignant transformation, triggers bidirectional interactions between HSPCs and antigen-specific $CD4^+$ T cells, causing stem cell proliferation, differentiation and specific exhaustion of aberrant HSPCs. In leukemia mouse models, this immunosurveillance mechanism effectively eliminates transformed HSPCs from the system, thereby preventing leukemia onset. Together, our data reveal a bidirectional interaction between HSPCs and $CD4^+$ T cells, demonstrating that HSPCs are not only passive receivers of immunological signals, but actively engage in adaptive immune responses to safeguard the integrity of the stem cell pool.

Introduction

Hematopoietic stem and progenitor cells (HSPCs) are the ultimate source of blood and immune cells, including antigen presenting cells (APCs) and T cells (Doulatov *et al.*, 2012; Eaves, 2015). In contrast to mature cell types, HSPCs are multipotent, long-lived and self-renew. The acquisition of genomic aberrations in HSPCs constitutes a major threat to the hematopoietic system, since genomic errors are passed on to daughter stem cells and eventually to the entire hematopoietic system, where they are maintained throughout life. In the elderly, the establishment of such clonally expanded populations carrying pre-leukemic mutations is a frequent event and associated with a high risk of malignant transformation to hematological cancers (Genovese *et al*., 2014; Jaiswal *et al*., 2014). To protect stem cells from damage induced by replicative stress and reactive oxygen species, HSPCs are maintained in a long-term quiescent and low metabolic state (van Galen *et al*., 2014; Walter *et al*., 2015; Ho *et al*., 2017). While inflammatory signals released during infections activate HSPCs to propel blood production, excessive exposure to inflammation induces replicative stress causing DNA damage and stem cell exhaustion (Essers *et al*., 2009; Sato *et al*., 2009; Walter *et al*., 2015; Zhang *et al*., 2016; Takizawa *et al*., 2017). $CD4^+$ regulatory T cells (Tregs) have been suggested to establish an immune privileged niche in the bone marrow maintaining stem cell quiescence, presumably by protecting stem cells from replicative stress induced by inflammatory insults (Fujisaki *et al.*, 2011; Hirata *et al.*, 2018). While several mechansisms have been described how stem cells are passively protected by their microenvironment to prevent the acquisition of damage, active safety mechanisms that specifically eliminate malignant HSPCs from the system remain unknown.

Professional APCs, such as B cells or mature dendritic cells (DCs), induce adaptive immune responses by presenting antigens via the major histocompatibility complex class II (MHC-II) to the T cell receptor of $CD4^+$ T cells (Neefjes *et al.*, 2011; Roche and Furuta, 2015). Microenvironmental factors, the maturation state of APCs and the expression of co-stimulatory molecules on APCs have been implicated in balancing immunogenic versus tolerogenic T cell responses (Wakkach *et al.*, 2003; Goodnow *et al.*, 2005; Jurewicz and Stern, 2019). Professional APCs constitutively express high levels of MHC-II (Steinman, 2007; Merad *et al.*, 2013; Roche and Furuta, 2015), whereas immature or non-professional APCs acquire antigen presentation activity only upon exposure to inflammatory signals associated with MHC-II up-regulation (Kambayashi and Laufer, 2014; Jakubzick, Randolph and Henson, 2017). The majority of other cell types are typically devoid of MHC-II expression and are not capable of priming $CD4^+$ T cells. Despite several studies reporting that MHC-II might be expressed on immature cells of the hematopoietic system (Russell and Engh, 1979; Fitchen, Foon and Cline, 1981; Sieff *et al*., 1982; Szer *et al*., 1985), HSPCs have not been considered capable of actively interacting with the adaptive immune system. Moreover, a systematic understanding of the MHC-II expression patterns is lacking and the functionality as well as the role of MHC-II-mediated antigen presentation in HSPCs during health and disease remains unexplored.

Here, we demonstrate that HSPCs constitutively present antigens via MHC-II. Upon presentation of immunogenic antigens, HSPCs directly interact with antigen-specific $CD4^+$ T cells, driving HSPC differentiation and extinction from the system. On the other hand, $CD4^+$ T cells adopt an immunoregulatory state preventing harmful pro-inflammatory bone marrow responses. This immunosurveillance mechanism effectively suppresses leukemia onset upon malignant transformation of HSPCs.

Results

Mouse HSPCs express the MHC-II antigen presenting machinery

To systematically explore the expression patterns of the MHC-II antigen presentation machinery in the hematopoietic system, we performed a series of analyses. First, global transcriptome datasets of mouse multipotent hematopoietic stem and progenitor cells (HSPCs) ($Lin^-Sca1^+cKit^+$ cells, LSKs) revealed high expression of genes encoding MHC-II molecules (*H2-Aa*, *H2-Ab1*, *H2-Eb1*), the related antigen loading machinery (*H2-Dma*, *H2-Dmb2*, *H2-Oa*, *H2-Ob*, *Cd74*) and *Ciita*, the master regulator of MHC-II gene expression (Steimle *et al.*, 1993, 1994) (Figure 1A). Targeted transcriptional profiling confirmed that MHC-II genes were highly expressed in mouse hematopoietic stem cells (HSCs) and multipotent progenitors (MPPs) 1-4 (see Methods) (Cabezas-Wallscheid *et al.*, 2014), together comprising the LSK compartment. These genes were gradually downregulated upon transition to committed progenitors that comprise the $Lineage^-Sca\text{-}1^-c\text{-}Kit^+$ (LS^-K) compartment (Figure 1B). To analyze MHC-II protein expression, we measured MHC-II surface expression levels across all major cell populations present in the mouse bone marrow and spleen by flow cytometry (Figures 1C, 1D, S1A and S1B). As expected, professional APCs expressed consistently high levels of MHC-II, non-professional APCs expressed MHC-II at heterogeneous levels, and non-APCs did not express MHC-II. Importantly, HSCs and MPPs showed prominent surface expression levels of MHC-II, which were gradually downregulated upon transition to committed progenitors of the LS^-K compartment, in line with our transcriptomic data. Notably, homeostatic levels of MHC-II molecules in HSCs and MPPs were only slightly lower as compared to professional APCs, but significantly higher when compared to any other population examined, including macrophages (Figures 1C, 1D, S1A and S1B). Transcript and protein levels of MHC-II genes were efficiently up-regulated in HSCs *in vivo* upon administration of bacterial lipopolysaccharide (LPS), recombinant type-I interferon, the viral mimetic polyinosinic:polycytidylic acid (pI:C) or following viral infection with MCMV (Figures 1C, 1D and S1A-S1C). Stimulation by LPS or pI:C treatment of mice enhanced expression of MHC-II surface levels in HSCs comparable to those observed in professional APCs, but had only negligible impact on non-APCs.

To unambiguously determine whether MHC-II expression marks HSCs with long-term self-renewal capacity, we separated lineage-depleted bone marrow solely based on MHC-II surface expression, followed by transplantation into lethally irradiated mice (Figures 1E, 1F, S1D and S1E). While MHC-II-negative bone marrow cells were not capable of repopulating all hematopoietic lineages efficiently, MHC-II-positive bone marrow cells reconstituted hematopoiesis long-term, demonstrating that MHC-II surface expression is an explicit feature of self-renewal capacity and therefore marks all functional HSCs.

Mouse HSPCs present antigens via MHC-II

To determine whether mouse HSPCs are capable of presenting antigens via MHC-II, we made use of the Y-Ae antibody, that recognizes the MHC-II-derived Eα $peptide_{52\text{-}68}$ when presented in the context of MHC-II $I\text{-}A^b$ haplotype (Murphy *et al.*, 1989; Rudensky *et al.*, 1991). Accordingly, in C57BL/6 mice, that display the $I\text{-}A^b$ haplotype but lack expression of Eα, exogenous Eα peptide can be used as foreign antigen to characterize antigen presentation capacities of cell populations *ex vivo*. While professional APCs efficiently presented the Eα peptide via MHC-II and non-APCs failed to do so, HSPCs presented MHC-II-restricted peptides

efficiently, suggesting that HSPCs can present exogenous peptides *ex vivo* (Figure 2A). In support of this, HSPCs efficiently incorporated and processed exogenously administered BODIPY-conjugated DQ-ovalbumin (DQ-OVA), a self-quenched conjugate that exhibits fluorescence upon cleavage, *ex vivo* and *in vivo* (Figure S2A-S2C).

To investigate whether HSPCs of naïve mice present self-antigens via MHC-II *in vivo*, we crossed BALB/C mice, which express Eα but exhibit the I-A^d haplotype, to C57BL/6 mice (I-A^b, Eα-negative). In mice of the F1 generation, MHC-II mediated self-antigen presentation can be assessed by the Y-Ae antibody, due to the expression of Eα in the presence of MHC-II molecules with I-A^b haplotype (Henri *et al.*, 2010) (Figure S2D). In line with previous reports, professional APCs displayed efficient MHC-II mediated presentation of Eα during homeostasis and upon LPS treatment *in vivo*, macrophages did not present Eα at homeostasis, but acquired strong antigen presentation capacity upon LPS treatment, and non-APCs showed no or highly restricted antigen presenting activity (Kambayashi and Laufer, 2014; Jakubzick, Randolph and Henson, 2017) (Figure 2B, 2C and S2E). Importantly, HSCs and MPPs exhibited significant antigen presentation of Eα at homeostasis, and efficiently increased antigen presenting capacity upon LPS treatment in an MHC-II restricted manner, suggesting that HSPCs constantly present self-peptides via MHC-II in naïve mice (Figure 2B, 2C and S2E).

To identify the length and origin of antigens presented by HSPCs, we performed immunoprecipitation of MHC-II molecules from HSPCs of naïve mice, followed by peptide elution and mass spectrometry (Figure 2D and 2E). We also included T cells and splenocytes, serving as negative and positive control of APCs, respectively. Enumeration and characterization of MHC-II eluted peptides revealed that peptides from HSPCs resembled those from splenocytes in number and length distribution, and considerably outnumbered peptides eluted from non-APCs (Figure 2D). The evaluation of detected peptides confirmed that predominantly abundant self-peptides are presented by HSPCs in naïve mice (Figure 2E, Supplementary Table 1). Together, these data demonstrate that HSPCs constitutively present self-antigens via MHC-II at homeostasis and further increase antigen presentation upon inflammation.

Antigen presenting HSPCs engage in bidirectional interactions with antigen-specific $CD4^+$ T cells

The main feature of APCs is the antigen-specific activation of $CD4^+$ T cells. To study whether HSPCs can interact with $CD4^+$ T cells in an antigen-specific manner, we made use of OT-II and 2D2 mice that express transgenic T cell receptors specifically recognizing the chicken ovalbumin ($OVA_{323-339}$) or myelin oligodendrocyte glycoprotein (MOG_{35-55}) peptides, respectively, when presented by MHC-II (Barnden *et al.*, 1998; Bettelli *et al.*, 2003). Co-cultures of multipotent HSPCs (LSKs) with naïve antigen-specific $CD4^+$ T cells resulted in efficient $CD4^+$ T cell activation and proliferation specifically in the presence of the respective peptides (Figures 3A, 3B, S3A-S3D). Notably, all populations of the LSK compartment, including HSCs and MPP1-4 induced antigen-specific $CD4^+$ T cell responses (Figure 3C). Since these populations also express similar levels of MHC-II and exhibit comparable presentation of endogenous antigens *in vivo* (see above), we used LSK cells in the majority of functional experiments that characterize antigen presentation of mouse multipotent HSPCs throughout this study. Importantly, blocking MHC-II abrogated HSPC-mediated activation of $CD4^+$ T cells, demonstrating that antigen-specific $CD4^+$ T cell activation is MHC-II dependent (Figure S3E).

While HSPCs efficiently activated CD4$^+$ T cells in the presence of processed peptides, they were also able to present antigens derived from OVA protein, albeit to a lesser extent if compared to DCs (Figure S3F). However, LPS-based inflammatory signals significantly enhanced the HSPC-mediated activation of CD4$^+$ T cells in the presence of OVA protein.

To determine whether HSPCs are capable of incorporating, processing and presenting exogenous antigens *in vivo*, we administered OVA protein to mice. Indeed, HSPCs isolated from OVA-injected mice were able to activate antigen-specific OT-II CD4$^+$ T cells *ex vivo* (Figure 3D), indicating their capability to process and present exogenous antigens *in vivo*. To confirm whether HSPCs were able activate CD4$^+$ T cells upon presentation of endogenous antigens, we co-cultured HSPCs from wild type or ovalbumin-expressing mice (CAG-OVA) with OT-II T cells. Indeed, OT-II T cells were specifically activated in the presence of HSPCs expressing OVA endogenously (Figure 3E). Together these experiments suggest that HSPCs are capable of activating CD4$^+$ T cells upon presentation of both endogenous and exogenous antigens via MHC-II.

Next, we investigated the impact of MHC-II mediated antigen presentation on HSPCs. In co-cultures, antigen-specific interactions with naïve CD4$^+$ T cells resulted in substantial proliferation of HSPCs (Figure 3F and S3H). Moreover, transwell assays demonstrated that direct contact between HSPCs and CD4$^+$ T cell cells is required for full cell cycle activation of HSPCs *ex vivo* (Figure S3I and S3J). To evaluate the mechanistic role of MHC-II in HSPC-T cell interactions *in vivo*, we generated mice carrying the tamoxifen-inducible recombinase CreERT2 under the control of the HSPC-specific SCL promoter, a loxP-flanked MHC-II allele (*H2-Ab*) and a loxP-flanked STOP sequence followed by the Enhanced Yellow Fluorescent Protein (YFP) (Figure 3G, see Methods). This enabled an efficient conditional deletion of MHC-II in HSPCs and their progeny (Figures S3K and S3L). Co-transfer of OVA-specific OT-II cells into tamoxifen-treated mice, followed by OVA immunization resulted in specific cell cycle induction of HSPCs that maintained physiological MHC-II levels, while MHC-II deficient HSPCs from the same mice did not respond to OVA treatment (Figures 3G and 3H). Together, these observations demonstrate that transient presentation of immunogenic antigens via MHC-II by HSPCs mediates bidirectional interactions with antigen-specific CD4$^+$ T cells, resulting in simultaneous activation of stem and T cells.

Sustained antigen presentation drives differentiation and elimination of HSPCs from the stem cell pool

To investigate the physiological relevance of our findings, we explored the long-term consequences of sustained presentation of immunogenic antigens by HSPCs as occurring during chronic infections or malignant transformation. For this purpose, we generated mice with chimeric hematopoietic systems by co-transplantation of equal numbers of wild type HSPCs and CAG-OVA HSPCs, constitutively presenting the foreign chicken OVA antigen, into lethally irradiated congenic mice (Figure 4A). In the absence of antigen-specific CD4$^+$ T cells, this resulted in a stable 50:50 chimerism of the two hematopoietic systems throughout primary and secondary transplantation, suggesting that the presentation of antigens in the absence of antigen-specific CD4$^+$ T cells does not affect hematopoiesis (Figure 4B). In contrast, upon co-transfer of OVA-specific OT-II CD4$^+$ T cells at the beginning of the primary transplantation (d0), OVA-expressing HSPCs were immediately removed from the system, resulting in a complete and specific engraftment failure of stem cells presenting the T cell-

recognized antigen (Figure 4B and 4C). If OT-II cells were co-transferred after stable engraftment of the two hematopoietic systems (d60 post transplantation), the chimerism was kept stable initially, but started dropping upon secondary transplantation. Importantly, also in this setting, antigen presenting HSPCs were efficiently decreased and eliminated after primary and secondary transplantation, respectively.

While antigen-specific $CD4^+$ T cells strongly expanded and accumulated in the bone marrow during stem cell exhaustion, antigen-specific $CD8^+$ T cells were not detected (Figures 4D, S4A and S4B), suggesting that the elimination of antigen presenting HSPCs was mediated by direct $CD4^+$ T cell interactions and not by secondary activation of cytotoxic $CD8^+$ T cells. Of note, loss of OVA-presenting HSPCs was associated with an increased myeloid-biased differentiation (Figure 4E). To determine whether differentiation is the main cause of elimination of antigen presenting stem cells, we first investigated the impact of antigen presentation on HSPCs differentiation. In co-cultures, antigen-specific interactions with $CD4^+$ T cells induced rapid differentiation of HSPCs into the myeloid lineage, associated with loss of *in vivo* stem cell potential as measured by bone marrow transplantations (Figures 4F-4I and S4C). Gene expression analyses confirmed the upregulation of differentiation programs in HSPCs and their progeny (Figure S4D). In line with this, co-transfer of OVA-loaded HSPCs with OVA-specific $CD4^+$ T cells into mice resulted in rapid differentiation of HSPCs *in vivo* (Figure 4J and 4K). Finally, transwell assays demonstrated that direct HSPC-$CD4^+$ T cell interactions are required to effectively drive HSPC differentiation (Figure S4E). Together, these data suggest that direct interactions with antigen-specific $CD4^+$ T cells drive differentiation and exhaustion of HSPCs that present the cognate immunogenic antigens via MHC-II, thereby irreversibly removing them from the system, while leaving unrecognized self-antigen presenting HSPCs unaffected.

Antigen-specific HSPC-$CD4^+$ T cell interactions promote an immune-privileged state

Inflammatory signals, such as those released during pro-inflammatory T cell responses, induce systemic HSPC proliferation (Essers *et al*., 2009; Baldridge *et al*., 2010; Walter *et al*., 2015). However, antigen presentation by HSPCs resulted in the specific activation and exhaustion of stem cells that actively present immunogenic antigens, while leaving self-antigen presenting HSPCs unaffected (see above), suggesting that HSPC-mediated T cell activation occurs in the absence of global pro-inflammatory bone marrow responses. Since naïve $CD4^+$ T cells can be polarized into pro-inflammatory or immunosuppressive T helper subsets depending on the properties of the APC and environmental factors (Zhu and Paul, 2010), we investigated the exact nature of HSPC-induced T cell polarization.

First, we characterized the APC properties of HSPCs. Gene expression analyses of HSPCs revealed low to intermediate expression of classical co-stimulatory molecules, but high surface presentation of the co-inhibitory molecule PD-L1 (Figure S5A and S5B). Moreover, the most highly expressed cytokine genes in HSPCs are *Ebi3* and *Il12a* (Figure S5C), forming together the suppressive cytokine IL-35 (Collison *et al*., 2007, 2010). Upon engagement with antigen-specific $CD4^+$ T cells, HSPCs further upregulated PD-L1, acquired features of myeloid-derived suppressor cells and expressed high levels of the immunoregulatory cytokines IL-10 and IL-27 (Figure S5D-S5H). Since high expression of immunoregulatory cytokines and co-inhibitory receptors by APCs are associated with the promotion of anti-inflammatory or regulatory T cell responses (Ness, Lin and Gordon, 2021), we investigated whether antigen

presentation by HSPCs might polarize $CD4^+$ T cells to an immunoregulatory state. Indeed, in contrast to $CD4^+$ T cells activated by other APCs, $CD4^+$ T cells activated by HSPCs acquired a unique state, characterized by high surface expression of co-inhibitory molecules, such as PD-L1 (Figures S6A and S6B). This was also the case for $CD4^+$ T cells activated by highly purified HSCs and MPP populations (Figure S6C). Global transcriptomic comparisons of $CD4^+$ T cells activated by HSPCs, in the following termed T_{HSCs}, with $CD4^+$ T cells activated by conventional DCs (T_{DCs}) confirmed that they acquired fundamentally distinct transcriptomic states, with T_{HSCs} adopting an immunoregulatory and anti-inflammatory phenotype (Figure 5A and 5B). Of note, the expression of the signature transcription factor of regulatory T cells (Tregs), *Foxp3,* remained absent upon HSPC-mediated T cell activation (Figure S6D). In contrast, an upregulation of the transcription factors *c-Maf* and *Prdm1* was observed, which act as master regulators of type 1 regulatory T (Tr1) cell differentiation and mediate the transcriptional induction of co-inhibitory gene modules in T cells (Chihara *et al.,* 2018; Zhang *et al.*, 2020) (Figures 5B and S6D). In line with this, T_{HSCs} up-regulated robust and sustained expression of the immune suppressive cytokine IL-10 and a co-inhibitory gene module comprising the co-inhibitory molecules PD-1 (*Pdcd1*), PD-L1 (*Cd274*), LAG3 (*Lag3*) and TIM3 (*Havcr2*) on the mRNA and protein level (Figures 5C, S6D-S6F). The expression of co-inhibitory molecules and signature Tr1 transcription factors in T_{HSCs} remained elevated upon resting, antigen-dependent or -independent re-stimulation and exposure to inflammatory molecules, suggesting that the regulatory phenotype is not due to a transient activation state, but rather reflects a stable state linked to differentiation (Figures S6G-S6J).

To evaluate whether T_{HSCs} acquired a functionally suppressive phenotype *ex vivo*, we performed suppression assays using canonical Tregs as control (Figure 5D-5G). In contrast to T_{DCs}, T_{HSCs} efficiently suppressed $CD4^+$ and $CD8^+$ T cell responses in an antigen-dependent and -independent manner (Figure 5D-5H). Moreover, T_{HSCs} reduced the cytotoxic activity of $CD8^+$ T cells and supported macrophage polarization to an anti-inflammatory M2 state (Figure 5I and 5J). Mechanistically, both the capacity of T_{HSCs} to suppress bystander T cells and to polarize macrophages to an M2 state was, at least partly, driven by IL-10 (Figure 5J and 5K), which is upregulated both in HSPCs and $CD4^+$ T cells upon bidirectional interactions (see above). Adoptive transfers of T_{HSCs} into mice effectively suppressed the response of naïve OT-II T cells to OVA immunizations, demonstrating the *in vivo* capacity of T_{HSCs} to dampen the immune system (Figure 5L).

In line with our *ex vivo* results, upon sustained interactions with CAG-OVA HSPCs *in vivo*, antigen-specific $CD4^+$ T cells acquired a PD-L1 high phenotype (Figure S6K). Both antigen-specific $CD4^+$ T cells and the CAG-OVA HSPC-derived bone marrow cells of mice in which HSPC-mediated antigen presentation occurred, adopted a functionally suppressive phenotype, confirming that sustained antigen presentation by HSPCs causes an overall immunoregulatory bone marrow response *in vivo* (Figures S6L and S6M).

Together, these findings demonstrate that antigen presentation by HSPCs to $CD4^+$ T cells triggers an immunoregulatory T cell state, causing HSPC and T cell activation while promoting an immune privileged environment to avoid harmful pro-inflammatory responses in the bone marrow.

Human HSPCs are antigen presenting cells

In order to investigate whether our findings in the mouse system can be translated to humans, we first analyzed bulk and single-cell transcriptome datasets of human HSPCs

(Novershtern *et al.*, 2011; Hay *et al.*, 2018; Pellin *et al.*, 2019). These analyses revealed high expression of genes encoding MHC-II (e.g. *HLA-DRA*, *HLA-DRB*) and the machinery related to antigen presentation via MHC-II (e.g. *HLA-DMA*, *HLA-DMB*, *CD74*) in HSCs and MPPs (Figure 6A, S7A and S7B). While the expression of MHC-II and its antigen presenting machinery was maintained throughout commitment of HSCs to lineages with APC function (DC, B cell and monocyte/macrophage lineages), it was gradually downregulated upon commitment to all other lineages (neutrophil, eosinophil/basophil/mast cell, erythroid, megakaryocytic lineages). We next performed a flow cytometric characterization of the cell surface expression of the MHC-II molecule HLA-DR across major hematopoietic compartments of the bone marrow from healthy donors. The results accurately recapitulated our findings from the mouse system, with no expression of HLA-DR in non-APCs, high expression in professional APCs, and robust, albeit slightly lower expression in HSPCs and early progenitors of the $CD34^+$ compartment (Figures 6B and 6C and S7C). To confirm that MHC-II marks human HSCs with long-term self-renewal capacity, we transplanted human bone marrow, separated based solely on HLA-DR expression, into sublethally irradiated immunodeficient mice (Figure 6D). 20 weeks post-transplant, HLA-DR-positive bone marrow cells gave rise to significantly higher levels of human multilineage engraftment compared to HLA-DR-negative bone marrow, suggesting that functional HSC activity is associated with MHC-II expression (Figure 6E).

To investigate whether human HSPCs are capable of presenting antigens via MHC-II, we made use of CytoStim, an antibody-based reagent that cross-links MHC-II of APCs with the T cell receptor of $CD4^+$ T cells, resulting in T cell activation. As expected, addition of CytoStim resulted in efficient activation of $CD4^+$ T cells in co-cultures with professional APCs, but had little or no effect in co-cultures with non-APCs (Figure 6F and 6G). In contrast, addition of CytoStim to co-cultures of $CD34^+$ HSPCs and $CD4^+$ T cells resulted in efficient T cell activation, which was comparable to DC-mediated T cell activation. To determine whether human HSPCs can activate $CD4^+$ T cells in an antigen-dependent manner, we made use of a pool of peptides frequently recognized by a small subset of antigen-experienced $CD4^+$ T cells (Figure 6H). According to our previous observations, APCs and HSPCs comparably activated $CD4^+$ T cells reactive to the peptides. Of note, similar to their mouse counterparts, human $CD4^+$ T cells activated by human $CD34^+$ HSPCs acquired an immunoregulatory phenotype associated with upregulation of co-inhibitory molecules, such as LAG3, PD-L1 and TIM3, as well as increased expression of the *IL10* gene and Tr1 associated transcription factors, suggesting a conserved mechanism from mouse to human (Figure 6I-6K). Collectively, these data suggest that human HSPCs, similar to their mouse counterparts, act as antigen presenting cells capable of interacting with $CD4^+$ T cells via MHC-II.

MHC-II mediated antigen presentation is associated with a stem-like state in AML

Acute myeloid leukemia (AML) is an aggressive hematological cancer characterized by the accumulation of immature blasts that originate from HSCs or myeloid progenitors. MHC-II has been described to be expressed in a heterogeneous manner in AML (Miale *et al.*, 1982; Newman *et al.*, 1983), and its deregulation has been linked to relapse after allogeneic stem cell transplantation (Christopher *et al.*, 2018; Toffalori *et al.*, 2019). However, neither a rationale for MHC-II expression heterogeneity, nor a link to APC capacity and clinical or biological features of AMLs have been established (Miale *et al.*, 1982; Mutis *et al.*, 1997, 1998; Costello *et al.*, 1999; Berlin *et al.*, 2015). In line with our previous findings in the healthy hematopoietic system, transcriptomic analyses of 523 leukemia samples of AML patients

revealed that high expression of the MHC-II antigen presentation machinery is associated with a transcriptomic state of stemness (Pölönen *et al.*, 2019) (Figure 7A). In accordance with this, flow cytometric analyses of 63 AML patients confirmed that high HLA-DR (MHC-II) surface expression identifies patients with stem-like or monocyte-like AMLs and marks immature stem-like populations within the leukemic blast hierarchy of individual patients (Figure 7B, 7C and S8A-S8C). To determine whether a stem-like state in human AML is indeed associated with functional APC capacities, we screened 23 human AML cell lines and categorized them based on their immunophenotype into stem- or mature-like (Figure S8D and S8E). In line with our observations in primary AMLs, stem-like AML cell lines expressed higher HLA-DR levels, displayed higher $CD4^+$ T cell activation and immunosuppressive polarization capacities, and subsequently underwent myeloid differentiation, suggesting that the above-described bidirectional interaction might also be operational in stem-like AML cells (Figure 7D-F and S8E).

Interestingly, human AMLs with genomic alterations capable of transforming only HSCs, such as *FLT3*-ITD AMLs (without *NPM1* alterations), displayed a transcriptomic state of stemness and expressed consistently high levels of the MHC-II machinery (Figure 7G). In contrast, AMLs with *NPM1* mutations (without *FLT3* alterations), capable of also transforming differentiated progenitors, displayed a more differentiated phenotype and lower expression of the MHC-II machinery. These data suggest that the leukemic cell origin might determine the APC capacity of the AML. To experimentally test this, we generated stem cell-derived AMLs and mature granulocyte progenitor-derived AMLs by transducing either mouse LSK or GMP populations with the oncogene *MLL-AF9*, followed by transplantation into recipient mice (Krivtsov *et al.*, 2006, 2013). In line with our hypothesis, stem cell-derived AMLs expressed more MHC-II and were significantly more efficient in inducing MHC-II-dependent, antigen-specific $CD4^+$ T cell responses, if compared to myeloid progenitor-derived AMLs (Figure 7H, S8F and S8G). Together, these data demonstrate that the state of differentiation, linked to the cellular origin of AML, impacts on the capability of the disease to interact with the adaptive immune system. Moreover, similar to their healthy counterparts, stem cell-like leukemia cells display most efficient APC function, which is lost during granulocytic differentiation.

MHC-II mediated interactions between transformed stem cells and antigen-specific $CD4^+$ T cells prevent leukemia onset

Since healthy and malignant stem cells displayed APC capacities, we investigated whether the above described mechanism driving differentiation and depletion of immunogenic antigen-presenting stem cells could serve as an immunosurveillance mechanism to prevent leukemia onset by eliminating transformed HSPCs. According to our hypothesis, mutations generating MHC-II restricted neoantigens in humans should be efficiently out-selected in stem-like AMLs, but not in differentiated leukemias that express low levels of MHC-II, such as $NPM1^{mut}$ AMLs. In line with this, the IDH1(R132H) mutation, generating a well-established MHC-II restricted neoepitope (Schumacher *et al.*, 2014), occurred almost exclusively in differentiated $NPM1^{mut}$ AML but not in more immature $NPM1^{wt}$ AMLs (Figure 7I). In contrast, the non-immunogenic IDH1(R132C) AMLs showed a comparable proportion of $NPM1^{mut}$ AMLs to a general AML cohort, supporting the hypothesis that immature HSPCs acquiring immunogenic aberrations presented via MHC-II are efficiently removed from the hematopoietic system in humans.

To experimentally validate this hypothesis, we mimicked a malignant transformation resulting in immunogenic neoantigen presentation by transforming OVA-expressing HSPCs with the oncogene *MLL-AF9*, followed by transplantation into mice in the presence or absence of OVA-specific OT-II $CD4^+$ T cells (Figure 7J). While mice rapidly developed leukemias in the absence of $CD4^+$ T cells that specifically recognize the malignant leukemia stem cells, in the presence of OT-II T cells, transformed HSPCs were efficiently removed, preventing leukemia formation and accumulation of leukemia cells in the bone marrow (Figure 7K and 7L). Similar to our observations in the healthy system, upon bidirectional interactions with leukemia stem cells *in vivo*, antigen-specific $CD4^+$ T cells expanded in the bone marrow and acquired a PD-L1 high phenotype resembling T_{HSCs} capable of preventing harmful pro-inflammatory bone marrow reactions (Figure 7M and 7N). In line with this, bystander bone marrow T cells remained in a homeostatic state in the presence of PD-L1 high antigen-specific $CD4^+$ T cells, but were highly activated in the absence of antigen-specific $CD4^+$ T cells (Figure 7O). Of note, while newly transformed stem cells were efficiently eliminated by interactions with $CD4^+$ T cells before disease onset, addition of antigen-specific $CD4^+$ T cells after the establishment of the disease, did not rescue the animals (Figure 7P, see discussion). Together, these data suggest that presentation of immunogenic antigens by transformed stem cells act as surveillance mechanism to remove malignant cells from the hematopoietic system thereby preventing leukemia onset.

Discussion

The acquisition of genomic aberrations in HSPCs is the main cause for the development of hematological malignancies. Accordingly, several passive protection mechanisms reduce the exposure of HSPCs to molecular, cellular and inflammatory stress, minimizing the risk for a malignant transformation (Essers *et al*., 2009; Sato *et al*., 2009; Fujisaki *et al.*, 2011; van Galen *et al*., 2014; Walter *et al*., 2015; Zhang *et al*., 2016; Ho *et al*., 2017). In addition, regulatory T cells have been implicated in maintaining HSC quiescence and establishing an immune privileged niche to further protect HSPC integrity (Zou *et al.*, 2004; Urbieta *et al.*, 2010; Fujisaki *et al.*, 2011; Pierini *et al.*, 2017; Hirata *et al.*, 2018). However, active mechanisms that specifically eliminate abberant HSPCs from the stem cell pool have not been described to date. Here, we demonstrate that mouse and human HSPCs continuously present antigens via MHC-II as a protective mechanism. While the presentation of harmless self-antigens during homeostasis is immunologically ignored, the presentation of immunogenic antigens results in a bidirectional interaction between antigen presenting HSPCs and antigen-specific $CD4^+$ T cells. Engagement with $CD4^+$ T cells triggers an immunoregulatory T cell response, as well as cell cycle entry and differentiation specifically of those HSPCs that present immunogenic antigens. This results in the rapid elimination of aberrant HSPCs from the stem cell pool, while actively creating an immunoregulatory state counter-acting pro-inflammatory bone marrow responses that would endanger the remaining healthy HSPCs.

All in all, our data demonstrate that MHC-II based antigen presentation by HSPCs acts an immunosurveillance mechanism operational both in mouse and human, providing a mechanistic understanding for the recent clinical findings that relapse after allogeneic stem cell transplantation is tightly associated with loss of MHC-II in AML (Christopher *et al.*, 2018; Toffalori *et al.*, 2019). These findings may also provide a potential explanation for the heterogeneous response of AMLs to immunotherapies (Liao *et al.*, 2019; Barrett, 2020; Vago and Gojo, 2020) and could serve to identify strategies for patient stratification. Boosting or

restoring MHC-II mediated antigen presentation might serve as a future therapeutic avenue to prevent AML relapse. Lastly, a deregulation of this immunoregulatory MHC-II-T cell axis might also result in loss of stem cell function as observed in acquired idiopathic aplastic anemia, an autoimmune disease caused by the immune-mediated destruction of HSCs. In this line, particular MHC-II haplotypes and loss of heterozygosity are associated with aplastic anemia susceptibility and response to immunosuppressive therapy (Nakao *et al.*, 1994; Nimer *et al.*, 1994; Saunthararajah *et al.*, 2002; Rehman *et al.*, 2009; Dhaliwal *et al.*, 2011; Liu *et al.*, 2016; Young, 2018).

Together, our study reveals so far unrecognized insights into antigen-specific bidirectional interactions between HSPCs and $CD4^+$ T cells, demonstrating that HSPCs are not only passive receivers of immunological signals, but actively engage in adaptive immune responses to safeguard the stem cell pool integrity.

Limitations of the study

While our data demonstrate that leukemic HSPCs are rapidly cleared upon presentation of immunogenic neoantigens via MHC-II during disease onset, the functional role of MHC-II in fully established leukemias remains more elusive. Since antigen presentation by HSPCs polarize $CD4^+$ T cells to an immunoregulatory state, it is well conceivable that fully established leukemias may hijack this mechanism to actively create an immune suppressive environment and evade immune clearance. In line with this, extensive immune suppression is frequently observed in AML (Vago and Gojo, 2020). Moreover, while we present clear evidence that antigen presentation by HSPCs and $CD4^+$ T cell polarization are highly conserved across species, we cannot exclude that specific aspects might differ from mouse to human.

Acknowledgements

We would like to thank J. Panten as well as the members of the Haas, Kuchroo and Trumpp labs for helpful discussions. We thank M. Eich and K. Hexel, T. Rubner F. Blum from the DKFZ flow cytometry, members of the DKFZ animal facility, and D. Kozoriz for their assistance. We thank L. Bunse and M. Platten for the MHC-II conditional knockout mouse model. This work was supported by a German Academic Scholarship Foundation (Studienstiftung des Deutschen Volkes) PhD fellowship (to A.S.), the Emmy Noether Fellowship RA3166/1-1 funded by the Deutsche Forschungsgemeinschaft (DFG) (to S.RA), the P01AI073748 and R01NS030843, funded by the National Institute of Health (NIH) (to V.K.K.), the SFB873, FOR2674 and FOR2033, funded by the DFG, the SyTASC consortium (Deutsche Krebshilfe) (all to A.T.), the Dietmar Hopp Foundation and the José Carreras Foundation for Leukemia Research (grant no. DCJLS 20R/2017) (both to A.T. and S.H.) and the LeukoSyStem consortium (BMBF) (to S.RA and S.H.).

Author Contributions

P.H.M., A.S. and D.V. performed the majority of experiments with help from A.B., M.A.A.M., S.L.L., E.S., C.L.T., C.H., P.S.W., D.E., K.O.D., N.C.C., E.D., F.P., A.P. and C.K.. M.G. performed the MHC-II immunopeptidomics experiment with help from D.V. and P.H.M., and conceptional input from S.H.. H.J.U. and A.S. performed MLL-AF9 mouse model experiments with conceptional input from S.A.A., P.H.M. and S.H.. P.H.M., F.G. and C.A. performed bioinformatic analysis with conceptional input from D.H. and S.H.. S.RE, C.R., S.RA, R.L., T.B., W.O., M.D.M., M.A.G.E., S.B.E., W.K.H., D.N., M.H., C.T., L.B. and C.M.T. provided clinical samples, data, conceptional input or other essential resources. S.H. and P.H.M. wrote the manuscript and prepared figures with conceptional input from A.T., V.K., A.S. and D.V., as well as all other authors. P.H.M. and S.H. designed the experimental setup with input from A.S. and D.V.. S.H. conceived the study with conceptional input from A.T., V.K.K, P.H.M., A.S. and D.V..

Declaration of interest

V.K.K. is a co-founder, has ownership interest, and is on the SAB of Celsius Therapeutics and Tizona Therapeutics.

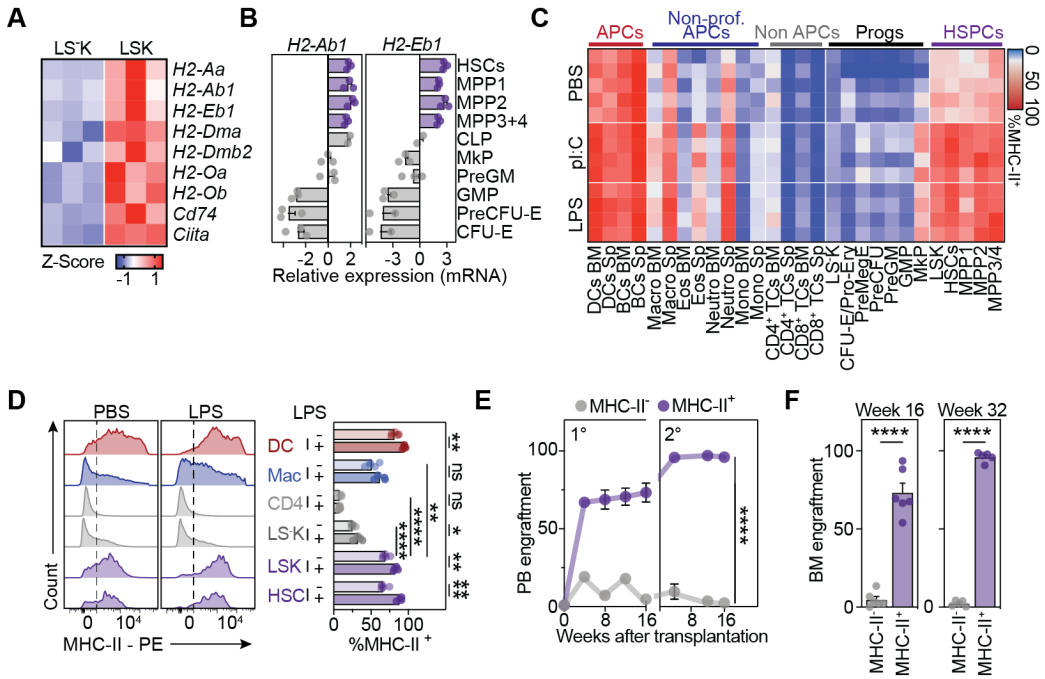

Figure 1. Mouse HSPCs express the MHC-II antigen presentation machinery.

See also Figure S1.

(**A**) z-scores of genes encoding components of the MHC-II antigen presentation machinery in mouse HSCs and MPPs (LSK) and committed progenitors (LS⁻K) derived from genome-wide RNA-Seq data (Klimmeck *et al.*, 2014), *n*=3.

(**B**) Relative gene expression of MHC-II genes across bone marrow populations measured by qPCR, *n*=2-3.

(**C**) Heatmap summarizing MHC-II surface measurements for bone marrow (BM) and spleen (Sp) populations by flow cytometry.

(**D**) MHC-II surface measurements by flow cytometry of indicated populations at homeostasis or 24 hours post LPS treatment. Representative histograms (left panels) and quantification (right panels), *n*=4-5. Dashed lines indicate thresholds for gating.

(**E** and **F**) Transplantation experiments of MHC-II$^{+/-}$ bone marrow populations. Lineage-negative bone marrow cells were sorted according to MHC-II expression and transplanted into lethally irradiated mice together with rescue bone marrow. Four months post transplantation, total bone marrow cells were transplanted into secondary recipients, *n*=4-6.

(**E**) Every 4 weeks, mice were bled and peripheral blood (PB) chimerism was measured by flow cytometry, *n*=4-6.

(**F**) Bone marrow chimerism was measured by flow cytometry at the endpoint of the primary (left) and secondary (right) transplantations, *n*=4-6.

Individual values are shown in A and C, means and SEM are depicted otherwise. No significance = ns, P<0.05 *, P<0.01 **, P<0.001 ***, P<0.0001 ****. Two-way ANOVA was performed in D as discovery test. If not stated otherwise, unpaired two-tailed t-tests were performed as post-hoc tests. When comparing paired cell populations within the same animal (D), paired two-tailed t-tests were performed. Two-way ANOVA was performed in E. Unpaired two-tailed t-tests were performed in F. In case of multiple comparisons, p-values were corrected according to Benjamini-Hochberg.

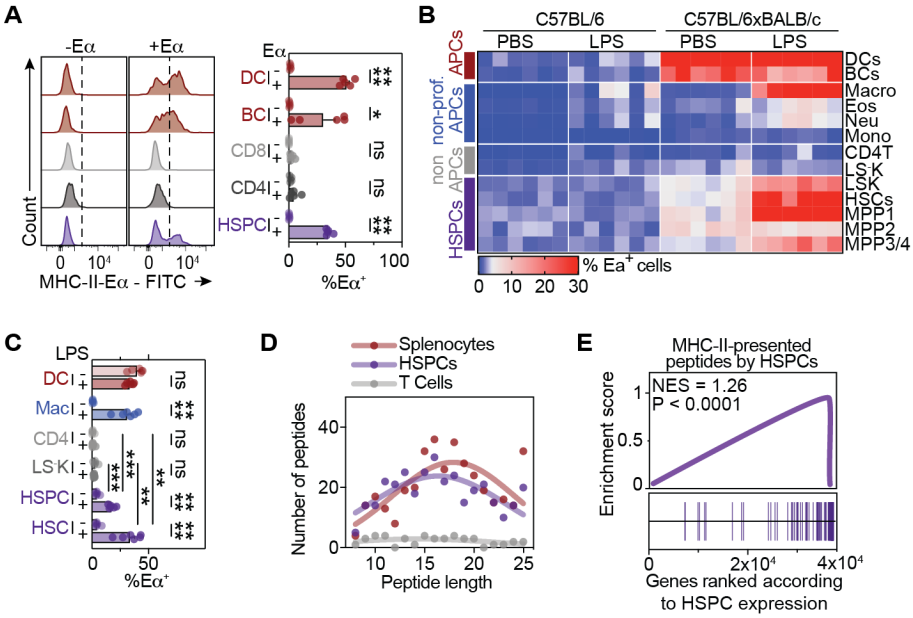

Figure 2. Mouse HSPCs present self-antigens via MHC-II.

See also Figure S2.

(**A**) *Ex vivo* antigen presentation assay of the indicated populations. Cells were cultured in the presence or absence of Eα peptide for three hours. The Y-Ae antibody was used to measure presentation of Eα via MHC-II. Representative histograms (left panels) and quantification (right panels), *n*=4. Dashed lines indicate thresholds for gating.

(**B** and **C**) *In vivo* antigen presentation assay. The Y-Ae antibody was used to measure presentation of Eα via MHC-II in C57BL/6xBALB/c mice and control C57BL/6 mice at homeostasis or 24 hours post LPS treatment. *n*=6. (**B**) Percentage of Eα presenting cells out of all depicted populations in naïve and LPS treated mice. (**C**) Quantification of selected populations. Only data for C57BL/6xBALB/c mice are depicted.

(**D** and **E**) Mass spectrometry analyses of peptides recovered from MHC-II of cKit$^+$ HSPCs and control populations (splenocytes and T cells). (**D**) MHC-II-eluted peptide size distribution for all three depicted populations. (**E**) Gene set enrichment analysis (GSEA) of MHC-II-presented antigens by HSPCs, related to the expression of the corresponding genes in the HSPC transcriptome (Klimmeck *et al.*, 2014).

Individual values are shown in B and D, means and SEM are depicted otherwise. No significance = ns, P<0.05 *, P<0.01 **, P<0.001 ***, P<0.0001 ****. One- (A) or two-way ANOVA (C) were performed as discovery tests. When comparing paired cell populations within the same animal (C), paired two-tailed t-tests were performed. If not stated otherwise, unpaired two-tailed t-tests were performed as post-hoc tests. In case of multiple comparisons, p-values were corrected according to Benjamini-Hochberg.

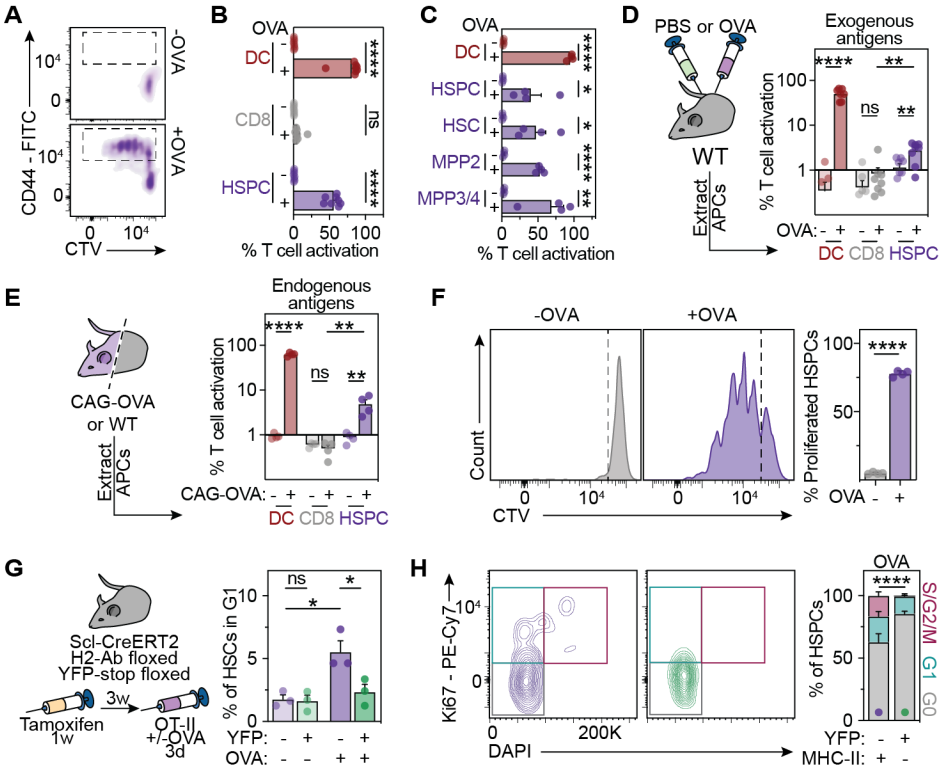

Figure 3. MHC-II mediates an antigen-specific bidirectional interaction between HSPCs and CD4⁺ T cells.

See also Figure S3.

(**A** and **B**) Evaluation of antigen presentation capacity by co-cultures of naïve OT-II CD4⁺ T cells with HSPCs (LSKs) and selected control populations in the presence or absence of OVA MHC-II-restricted peptide after 72 hours of co-culture, *n*=8. (**A**) Representative histograms of CD44 expression and cell trace violet (CTV). Dashed squares indicate thresholds for gating of activated T cells. (**B**) Quantification of T cell activation gated as described in (A).

(**C**) T cell activation assays for different HSPC subpopulations ($2.5x10^3$ cells) as in 3A, *n*=4.

(**D**) *In vivo* antigen presentation assay for exogenous antigens. One hour post administration of PBS or OVA protein to mice, $4x10^4$ CD8⁺ T cells, DCs or LSKs were isolated and co-cultured with naïve OT-II CD4⁺ T cells in the absence of exogenous OVA peptide. Left, illustration of experimental approach. Right, quantification of T cell activation, *n=8*.

(**E**) *In vivo* antigen presentation assay for endogenous antigens. HSPCs were isolated from CAG-OVA mice and from control mice. Antigen presenting capacity was read out by co-culture with OT-II CD4⁺ T cells in the absence of exogenous OVA peptide. Left, illustration of experimental approach. Right, quantification of T cell activation, *n=4*.

(**F**) Impact of antigen presentation on HSPC proliferation. Co-cultures with OT-II CD4⁺ T cells were performed as previously descibed. Proliferation of HSPCs was read out by CTV dilution 72 hours post co-culture. Dashed lines represent the gating of divided cells. Representative plots (left panels) and quantification (right panel), *n*=4.

(**G** and **H**) *In vivo* antigen-specific HSPC-T cell interaction promotes HSPC cell cycle entry. (**G**) Experimental scheme (left), Scl-CreERT2 H2-Ab floxed YFP-stop floxed mice were injected daily with tamoxifen during five days and three weeks, OT-II CD4+ T cells and OVA were injected three days prior to readout. Subsequently, HSPC cell cycle status was analyzed by flow cytometry as follows, G0, $Ki67^{-}DAPI^{low}$; G1, $Ki67^{+}DAPI^{low}$, S/G2/M, $Ki67^{+DAPImid/high}$. (Right) Comparison of YFP⁺ and YFP⁻ HSCs from Cre⁺ mice treated or not with ovalbumin, *n*=3. (**H**)

representative plots (left) and quantification (right) of $YFP^{+}MHC\text{-}II^{-}$ and $YFP^{-}MHC\text{-}II^{+}$ HSPCs from Cre^{+} mice treated with ovalbumin, *n*=5.
Means and SEM are depicted. No significance = ns, P<0.05 *, P<0.01 **, P<0.001 ***, P<0.0001 ****. One- (B, C) or two-way ANOVA (D, E, G and H) were performed as discovery tests. When comparing paired cell populations within the same animal (G), paired two-tailed t-tests were performed. If not stated otherwise, unpaired two-tailed t-tests were performed as post-hoc tests. In case of multiple comparisons, p-values were corrected according to Benjamini-Hochberg.

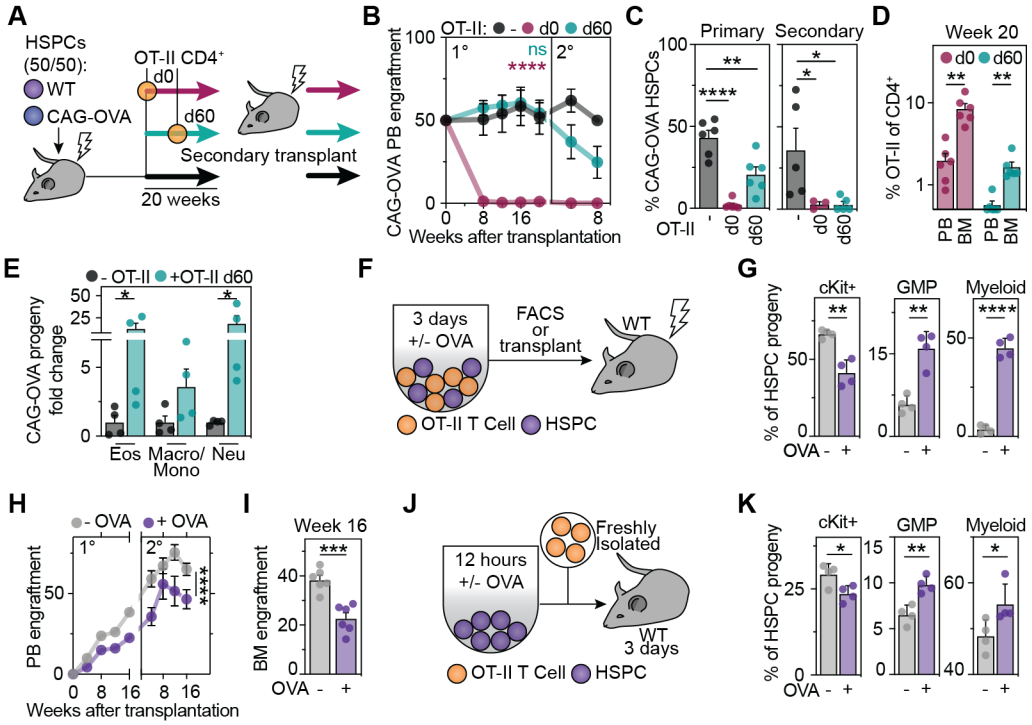

Figure 4. Sustained presentation of immunogenic antigens drives differentiation and exhaustion of HSPCs.

See also Figure S4.

(**A**-**E**) Sustained *in vivo* interactions between antigen presenting HSPCs and antigen-specific CD4$^+$ T cells trigger HSPC differentiation and exhaustion.

(**A**) Experimental scheme. WT or CAG-OVA HSPCs were sorted and co-transplanted in equal ratios into irradiated WT recipients with or without OT-II T cells at day 0 or day 60 post bone marrow reconstitution. 20 weeks post transplantation, mice were sacrificed, the bone marrow was analyzed and total bone marrow was re-transplanted into secondary recipients.

(**B**) Blood was taken from recipient mice every 4 weeks and the percentage of CAG-OVA progeny in peripheral blood was determined, *n*=4-6.

(**C**) Bone marrow chimerism was measured by flow cytometry at the endpoint of the primary (left) and secondary (right) transplantations, *n*=4-6.

(**D**) Percentage of OT-II CD4$^+$ T cells from the total CD4$^+$ T cell compartment in recipient mice after 20 weeks, *n*=6.

(**E**) Lineage-output upon HSPC-T cell interactions *in vivo*. Percentage of mature hematopoietic lineages generated by CAG-OVA cells 20 weeks after transplantation in the presence or absence of OT-II T cells transferred 60 days post initial transplantation. Fold change of the percentages relative to no OT-II injection is depicted, *n*=4.

(**F**-**I**) Impact of antigen presentation on HSPC differentiation.

(**F**) Experimental scheme. Co-cultures between HSPCs and OT-II T cells were performed as previously described in the presence and absence of ovalbumin, and analyzed by flow cytometry (**G**) or transplanted into lethally irradiated mice (**H** and **I**).

(**G**) Numbers of cKit$^+$, GMP (cKit$^+$CD16/32$^+$) or myeloid (cKit$^-$CD16/32$^+$ and CD11b$^+$) populations were quantified from the HSPC progeny, *n*=4.

(**H**) Peripheral blood engraftment over time of primary and secondary transplantation, *n*=6.

(**I**) Bone marrow engraftment at week 16, *n*=6.

(**J** and **K**) *In vivo* impact of antigen presentation on HSPCs.

(**J**) Experimental scheme. Sorted HSPCs (LSKs) were cultured in the presence or absence of OVA peptide for 12 hours and adoptively co-transferred with freshly sorted naïve OT-II $CD4^+$ T cells in untouched WT mice.
(**K**) 3 days post transfer, numbers of $cKit^+$, GMP ($cKit^+CD16/32^+$) or myeloid (cKit-$CD16/32^+$ and $CD11b^+$) populations were quantified of the HSPC progeny.
Means and SEM are depicted. No significance = ns, P<0.05 *, P<0.01 **, P<0.001 ***, P<0.0001 ****. One-way ANOVA (C, D and E) was performed as discovery tests. Two-way ANOVA was used in B and H. If not stated otherwise, unpaired two-tailed t-tests were performed as post-hoc tests. In case of multiple comparisons, p-values were corrected according to Benjamini-Hochberg.

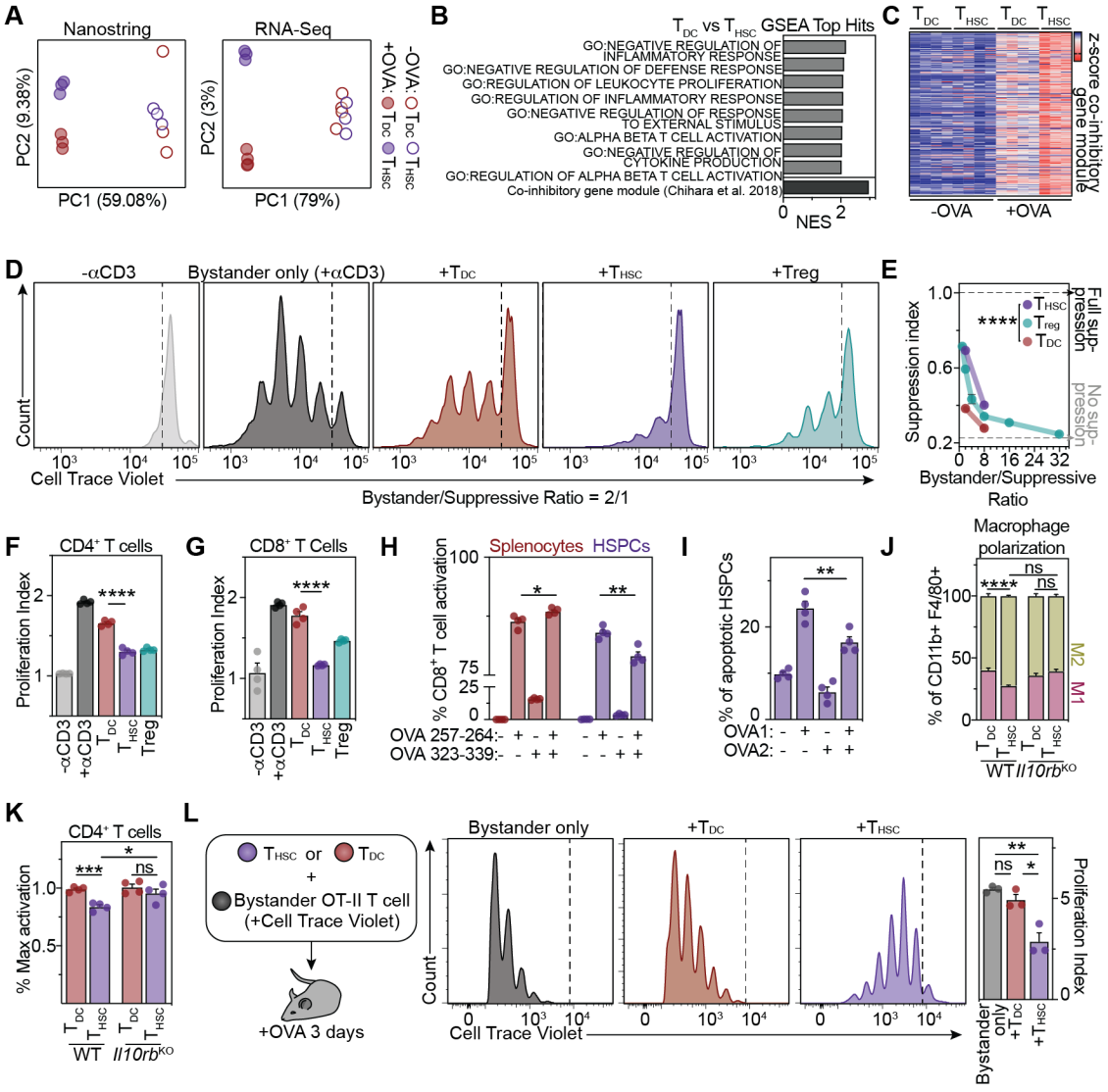

Figure 5. HSPC-mediated antigen-presentation induces a suppressive phenotype in CD4⁺ T cells.

See also Figure S5 and S6.

(**A**) Nanostring (left) and RNA-Seq (right) gene expression profiling of OT-II CD4⁺ T cells activated by HSPCs (T_{HSCs}) or dendritic cells (T_{DCs}) for 72 hours in the presence or absence of OVA peptide. Principle component analyses (PCA) was performed, *n*=3-4.

(**B**) Gene set enrichment analyses (GSEA) was performed using the RNA-Seq data from (A), comparing T_{HSCs} and T_{DCs}. Normalized enrichment score (NES) of the top T_{HSC}-enriched gene sets is represented.

(**C**) Heatmap representing normalized RNA-Seq gene expression from (A) of the co-inhibitory gene module (Chihara *et al.,* 2018).

(**D**-**F** and **K**) *Ex vivo* CD4⁺ T cell suppression assays. T_{HSCs} and T_{DCs} were generated as previously described, followed by 2 days of rest in the absence of the peptide. T_{HSCs}, T_{DCs} and freshly isolated Tregs were then co-cultured in different ratios with CTV-stained bystander/responder WT or *Il10rb*$^{-/-}$ naïve CD4⁺ T cells and supporting CD3^{-}CD19^{-} splenocytes in the presence or absence of activator αCD3 antibody for 72 hours. (**D**) Representative plots from the 1:2 suppressive/bystander naïve CD4⁺ T cells condition. Dashed line indicates non-

proliferated bystander T cells. (**E**) Suppression index (see Methods) is depicted for all investigated bystander/suppressive ratios, *n*=4. (**F**) Proliferation index of responder $CD4^+$ T cells is depicted for the 1:2 ratio, *n*=4.

(**G**) *Ex vivo* $CD8^+$ T cell suppression assays. T_{HSCs} and T_{DCs} were generated as previously desecribed, followed by 2 days of rest in the absence of peptide. T_{HSCs}, T_{DCs} and freshly isolated Tregs were then co-cultured in a 1:2 ratio with CTV-stained bystander/responder naïve $CD8^+$ T cells and supporting $CD3^-CD19^-$ splenocytes in the presence or absence of activator αCD3 antibody for 72 hours. Quantification of the proliferation of responder $CD8^+$ T cells is depicted, *n*=4.

(**H** and **I**) *Ex vivo* antigen specific $CD8^+$ T cell cytotoxicity assay. CTV-labelled naïve OT-I $CD8^+$ T cells were co-cultured with naïve OT-II $CD4^+$ T cells and HSPCs or splenocytes in the presence or absence of the MHC-I- and/or MHC-II-restricted OVA peptides for 72 hours, *n*=4. (**H**) OT-I T cell activation was measured by flow cytometry as previously described for $CD4^+$ T cells. (**I**) Cytotoxicity was quantified by assessing annexin V positivity by flow cytometry. OVA1: OVA 257-264, OVA2: OVA 323-339.

(**J**) *Ex vivo* macrophage polarization assay. T_{HSCs} and T_{DCs} were generated as previously described, followed by 2 days of rest in the absence of peptide. Subsequently, cells were co-cultured with $CD11b^+SSC^{low}$ WT (left) or *Il10rb*$^{-/-}$ (right) monocytes/macrophages and activator αCD3/αCD28 beads for 24 hours. Quantification of $F4/80^+$MHC-II^+ (M1) and $F4/80^+CD206^+$ (M2) macrophages is depicted, *n*=4.

(**K**) Effect of IL-10 on the $CD4^+$ T cell suppressive capacity of T_{HSCs}. Activation of WT (left) or *Il10rb*$^{-/-}$ (right) bystander T cells in the presence of T_{HSCs} relative to the presence of T_{DCs} in a 1:2 suppressive:bystander ratio. Values are normalized to the T_{DC} condition for each mouse model. *n*=4.

(**L**) *In vivo* suppression assay. T_{HSCs} and T_{DCs} were generated as in Figure 3A and adoptively co-transferred with CTV-labelled bystander naïve OT-II $CD4^+$ T cells in a ratio of 1:8 to WT mice. Bystander T cells were analyzed 3 days post OVA administration to mice. Representative plots (left panels) and quantification (right panels), *n*=3 are depicted.

Individual values are shown in A and C, means and SEM are depicted otherwise. No significance = ns, P<0.05 *, P<0.01 **, P<0.001 ***, P<0.0001 ****. One- (F, G, H, I, L) or two-way ANOVA (K) were performed as discovery test. Two-way ANOVA was performed in E and J. If not stated otherwise, unpaired two-tailed t-tests were performed as post-hoc tests. In case of multiple comparisons, p-values were corrected according to Benjamini-Hochberg.

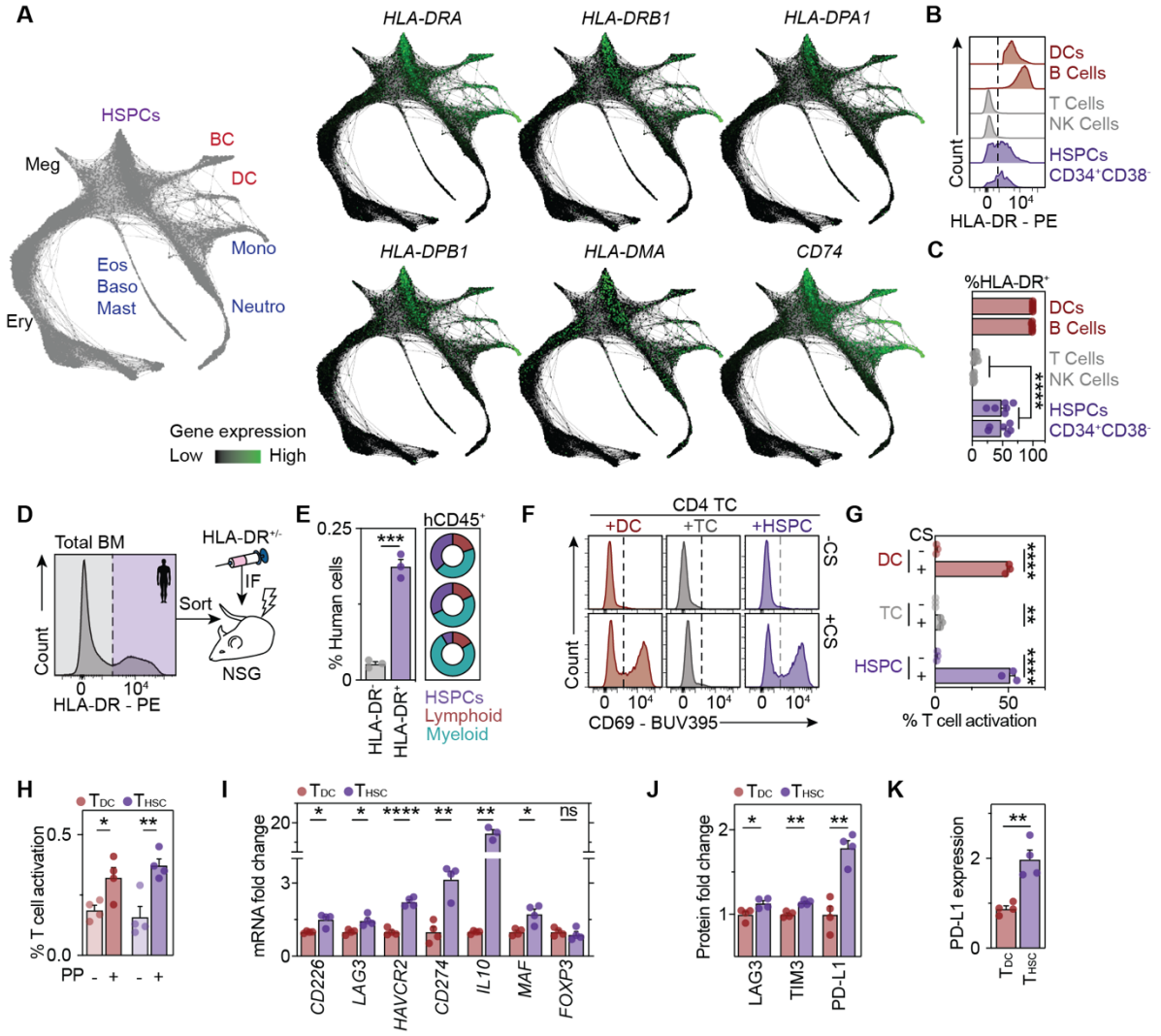

Figure 6. Human HSPCs act as antigen presenting cells.

See also Figure S7.

(**A**) scRNA-Seq across human HSPC differentiation trajectories displayed in a SPRING plot to visualize the differentiation trajectories (see Pellin *et al.*, 2019). Lineage annotation (left) and MHC-II gene expression patterns (right) are depicted.

(**B**) HLA-DR (MHC-II) surface measurements by flow cytometry of selected populations. Representative plots, *n*=6. Dashed lines indicate thresholds for gating.

(**C**) Quantification of HLA-DR$^+$ (MHC-II) surface measurements by flow cytometry of selected populations from bone marrow aspirates of healthy donors, *n*=6.

(**D** and **E**) Xenotransplantation experiments of HLA-DR bone marrow populations. (**D**) Total human bone marrow from 3 healthy donors was sorted based on HLA-DR expression and transplanted into sub-lethally irradiated NSG mice. *n*=4.

(**E**) Four months post transplantation, human CD45$^+$ cells in the bone marrow (left) and multilineage engraftment (right) were quantified. Each donut plot represents average engraftment levels per donor.

(**F-H**) T cell activation assays. Human bone marrow HSPCs (Lin$^-$CD34$^+$), dendritic cells (DCs) or T cells from peripheral blood (PB) were co-cultured with CTV-labeled naïve CD4$^+$ T cells in the presence or absence of CytoStim (CS, **F** and **G**) or an MHC-II-restricted peptide pool (PP, **H**) for 72 hours. Representative plots (**F**) and quantification of T cell activation (**G** and **H**), *n*=3-4. Dashed lines indicate thresholds for gating of activated T cells.

(**I**) qPCR analyses of $CD4^+$ T cells activated by HSPCs (Lin^-CD34^+) (T_{HSCs}) or dendritic cells (DCs) (T_{DCs}) in the presence of CytoStim as in 6F. Gene expression is presented relative to T_{DCs}, *n*=4.
(**J** and **K**) FACS analyses of human T_{HSCs} and T_{DCs}. T_{HSCs} and T_{DCs} were generated as in 6F. Protein expression is presented relative to T_{DCs}, *n*=4.
Means and SEM are depicted in all bar-plots. No significance = ns, P<0.05 *, P<0.01 **, P<0.001 ***, P<0.0001 ****. One-way ANOVA was performed in C, G, H, I and J as discovery test. Unpaired two-tailed t-tests were performed as post-hoc tests. In case of multiple comparisons, p-values were corrected according to Benjamini-Hochberg.

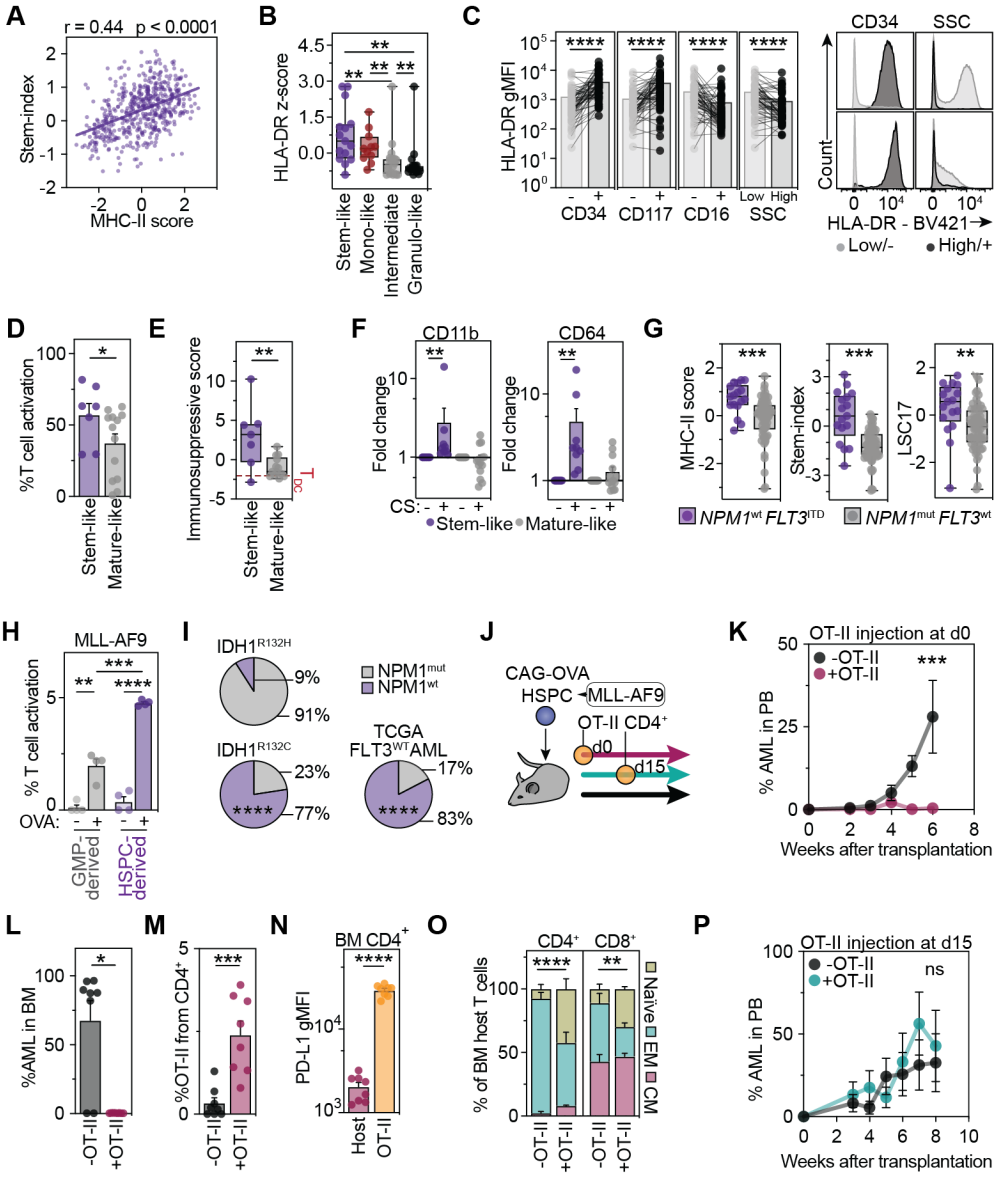

Figure 7. MHC-II-mediated neoantigen presentation of HSPCs protects from leukemia onset.
See also Figure S8.

(**A**) Stemness correlates with MHC-II expression in AML. Sum of scaled MHC-II gene expression and stem cell scores for AMLs from (Pölönen *et al.*, 2019) are depicted, *n*=523. Each dot represents an individual AML patient.

(**B** and **C**) AML patients were analyzed with EuroFlow panels by flow cytometry and stratified into the indicated groups based on clustering and corresponding indices summarizing expression of stem cell, granulocyte or monocyte markers across patient clusters (see Methods).

(**B**) HLA-DR surface expression in the different AML groups, *n*=63.

(**C**) HLA-DR geometric mean fluorescence intensity within blast sub-compartments positive or negative for representative stem (CD34 and CD117) or mature (CD16 and SSC) markers (left), *n=63*. Representative flow cytometry histograms of $CD34^{+/-}$ or $SSC^{high/low}$ populations from different AML patients (right).

(**D**) AML cell line T cell activation screen. 23 AML cell lines were characterized as stem-like or mature like based on their surface markers and co-cultured with human PB $CD4^{+}$ T cells in the

presence or absence of CytoStim (CS) for 72 hours. T cell activation was measured as previously described, *n*=23.

(**E**) Stem-like AML promotes an immunosuppressive phenotype on $CD4^+$ T cells. Surface expression of LAG3, PD-L1 and TIM3 on activated $CD4^+$ T cells was measured by flow cytometry, z-scored and combined to obtain an immunosuppressive score. Red dashed line represents the value of T_{DCs} educated concomitantly, *n*=23.

(**F**) Myeloid marker upregulation in stem-like AML upon T cell activation. CD11b (left) and CD64 (right) surface expression on AML cell lines after co-culture with and without CS measured by flow cytometry. Expression is presented relative to the unstimulated (CS-) value of each cell line, *n*=23.

(**G**) Sum of scaled MHC-II related genes (left) or stem cell scores (Ng *et al.*, 2016) (right, see Methods) in AML patients segregated based on NPM1 and FLT3 mutational state (Kohlmann *et al.*, 2010), *n*=78.

(**H**) Antigen presentation assays of HSC- and GMP-derived MLL-AF9 leukemia. Leukemias were induced by transduction of mouse LSK and GMP populations and transplantation into mice. Antigen presentation capacity was assessed by co-culture of leukemic cells with naïve $CD4^+$ OT-II T cells for 72 hours in the presence or absence of OVA peptide, *n=4*.

(**I**) Immunogenic mutations are highly depleted in stem-like $NPM1^{wt}$ AMLs if compared to differentiated $NPM1^{mut}$ AMLs. Proportion of $NPM1^{wt}$ or $NPM1^{mut}$ co-occurrence with immunogenic $IDH1^{R132H}$ (*n*=33), not immunogenic $IDH1^{R132C}$ (*n*=31) and $FLT3^{wt}$ AMLs (*n*=144). Original data from (Ley *et al.*, 2013; Falini *et al.*, 2019).

(**J**-**P**) Stem cell-derived leukemia antigen presentation impacts on disease onset.

(**J**) Experimental scheme. MLL-AF9 AML was induced in CAG-OVA HSPCs as previously described (see Methods) and injected in sublethally irradiated mice in the presence or absence of OT-II T cells at the day 0 (K-O) or 2 weeks post transplantation (P).

(**K** and **P**) AML expansion over time in the peripheral blood. Percentage of AML cells is indicated, *n=5-8*.

(**L**) Percentage of AML cells in bone marrow is indicated at the endpoint, *n=8*.

(**M**) Percentage of OT-II $CD4^+$ T cells in bone marrow is indicated at the endpoint, *n=8*.

(**N**) PD-L1 expression and bystander $CD4^+$ T cells in the bone marrow measured by flow cytometry is indicated, *n*=8.

(**O**) Adaptive immune microenvironment inflammatory state in the presence or absence of AML antigen specific responses. $CD4^+$ (left) and $CD8^+$ (right) host naïve ($CD44^-CD62L^+$), effector memory (EM, $CD44^+CD62L^-$) and central memory (CM, $CD44^+CD62L^+$) quantification, *n=8*.

Individual values are shown in A. Minimum to maximum are depicted in E and G, means and SEM are depicted otherwise. No significance = ns, P<0.05 *, P<0.01 **, P<0.001 ***, P<0.0001 ****. Two-way ANOVA (H) or Kruskal-Wallis (B and F) were performed as discovery tests. Linear regression analysis was performed in A. Chi-squared tests were performed in I. Two-way ANOVA was performed in K, O and P. Unpaired Mann-Whitney test was performed in B, D, E, G and L. Paired Mann-Whitney test was performed in C and F. If not stated otherwise, unpaired two-tailed t-tests were performed as post-hoc tests. In case of multiple comparisons, p-values were corrected according to Benjamini-Hochberg.

795 # STAR Methods

796

797 ## KEY RESOURCES TABLE

798

REAGENT or RESOURCE	SOURCE	IDENTIFIER
Mouse Antibodies		
Anti-mouse B220 FITC	ThermoFisher	Clone:RA3-6B2
Anti-mouse B220 AF700	ThermoFisher	Clone:RA3-6B2
Anti-mouse B220 APC-Cy7	ThermoFisher	Clone:RA3-6B2
Anti-mouse CD105 BV421	ThermoFisher	Clone:MJ7/18
Anti-mouse CD117 BV711	BioLegend	Clone:2B8
Anti-mouse CD117 PE	ThermoFisher	Clone:2B8
Anti-mouse CD117 PE-Cy5	BioLegend	Clone:2B8
Anti-mouse CD11b FITC	ThermoFisher	Clone:M1/70
Anti-mouse CD11b AF700	ThermoFisher	Clone:M1/70
Anti-mouse CD127 PE	BioLegend	Clone:A7R34
Anti-mouse CD150 PE-Cy5	ThermoFisher	Clone:TC15-12F12.2
Anti-mouse CD16/32 AF700	ThermoFisher	Clone:93
Anti-mouse CD16/32 APC	ThermoFisher	Clone:93
Anti-mouse CD19 APC	BioLegend	Clone:6D5
Anti-mouse CD206 FITC	BioLegend	Clone:C068C2
Anti-mouse CD25 BV785	BioLegend	Clone:PC61
Anti-mouse CD25 APC	BioLegend	Clone:PC61
Anti-mouse CD274 (PD-L1) BV711	BioLegend	Clone:10F.9G2
Anti-mouse CD274 (PD-L1) PE	BioLegend	Clone:10F.9G2
Anti-mouse CD279 (PD-1) APC	ThermoFisher	Clone:J43
Anti-mouse CD34 PE	BD	Clone:RAM34
Anti-mouse CD3e FITC	ThermoFisher	Clone:17A2
Anti-mouse CD3e	BioXCell	Clone:145-2C11
Anti-mouse CD4 BUV805	BD	Clone:GK1.5
Anti-mouse CD4 FITC	ThermoFisher	Clone:GK1.5
Anti-mouse CD4 AF700	ThermoFisher	Clone:GK1.5
Anti-mouse CD4 APC-Cy7	BioLegend	Clone:GK1.5
Anti-mouse CD41 APC	BioLegend	Clone:MWReg30
Anti-mouse CD41 FITC	BD	Clone:MWReg30
Anti-mouse CD44 FITC	ThermoFisher	Clone:IM7
Anti-mouse CD45 Pacific Blue	BioLegend	Clone:30F11
Anti-mouse CD45.1 BUV395	BD	Clone:A20
Anti-mouse CD45.1 BV606	BioLegend	Clone:A20
Anti-mouse CD45.1 PE	ThermoFisher	Clone:A20
Anti-mouse CD45.1 PE-Cy5	ThermoFisher	Clone:A20
Anti-mouse CD45.2 FITC	ThermoFisher	Clone:104
Anti-mouse CD45.2 APC-Cy7	ThermoFisher	Clone:104
Anti-mouse CD48 BUV395	BD	Clone:HM48-1
Anti-mouse CD48 APC	ThermoFisher	Clone:HM48-1
Anti-mouse CD48 Pacific Blue	BioLegend	Clone:HM48-1
Anti-mouse CD69 PE-Cy5	BioLegend	Clone:H1.2F3
Anti-mouse CD8 BUV395	BD	Clone:53-6.7
Anti-mouse CD8 FITC	ThermoFisher	Clone:53-6.7
Anti-mouse CD8 AF700	ThermoFisher	Clone:53-6.7
Anti-mouse CD84 PE	BioLegend	Clone:mCD84.7

Anti-mouse CD90.1 FITC	BioLegend	Clone:OX7
Anti-mouse F4/80 BV421	ThermoFisher	Clone:BM8
Anti-mouse Gr-1 FITC	ThermoFisher	Clone:RA3-6B2
Anti-mouse Gr-1 AF700	ThermoFisher	Clone:RA3-6B2
Anti-mouse Ki67 PE-Cy7	BD	Clone:B56
Anti-mouse Lag3 APC-Cy7	ThermoFisher	Clone:C9B7W
Anti-mouse MHC-II (I-A/I-E)	BioXCell	Clone:M5/114.15.2.
Anti-mouse MHC-II (I-A/I-E) BV785	BioLegend	Clone:M5/114.15.2.
Anti-mouse MHC-II (I-A/I-E) PE	BioLegend	Clone:M5/114.15.2.
Anti-mouse IL-10 PE	BioLegend	Clone:JES5-16E3
Anti-mouse Sca-1 APC-Cy7	BD	Clone:D7
Anti-mouse SiglecF Pacific Blue	BD	Clone:E50-Z440
Anti-mouse SiglecH PE	ThermoFisher	Clone:eBio440c
Anti-mouse TCR-b PE-Cy7	Biolegend	Clone:H57-597
Anti-mouse Ter119 FITC	ThermoFisher	Clone:Ter-119
Anti-mouse Ter119 AF700	ThermoFisher	Clone:Ter-119
Anti-mouse Tim3 APC	BioLegend	Clone:5D12
Anti-mouse I-Ab-Ea FITC	ThermoFisher	Clone:Y-Ae
Anti-mouse I-Ab-Ea Biotin	ThermoFisher	Clone:Y-Ae
Anti-human CD3 BUV395	BD	Clone:UCHT1
Anti-human CD4 APC	BD	Clone:561844
Anti-human CD4 BUV805	ThermoFisher	Clone:SK3
Anti-human CD8 APC	BD	Clone:RPA-T8
Anti-human CD11b APC	BD	Clone:ICRF44
Anti-human CD11c BV605	BD	Clone:563929
Anti-human CD11c Pe-Cy7	BioLegend	Clone:3.9
Anti-human CD19 APC	ThermoFisher	Clone:HIB19
Anti-human CD19 APC-Cy7	BioLegend	Clone:H1B19
Anti-human CD19 BV786	BioLegend	Clone:H1B19
Anti-human CD20 APC	BD	Clone:2H7
Anti-human CD25 PE-Cy7	BioLegend	Clone:BC96
Anti-human CD33 BV421	BioLegend	Clone:WM53
Anti-human CD34 APC-Cy7	ThermoFisher	Clone:H1B19
Anti-human CD38 A700	ThermoFisher	Clone:HIT2
Anti-human CD41a APC	BioLegend	Clone:HIP8
Anti-human CD45 APC	BioLegend	Clone:HI30
Anti-human CD45 PE	ThermoFisher	Clone:HI30
Anti-human CD45RA FITC	BioLegend	Clone:HI100
Anti-human CD45RO FITC	BioLegend	Clone:UCHL1
Anti-human CD49b FITC	BioLegend	Clone:PIE6-C5
Anti-human CD49f PE-Cy7	ThermoFisher	Clone:GoH3
Anti-human CD56 APC	BD	Clone:B159
Anti-human CD56 Alexa Fluor 488	BD	Clone:B159
Anti-human CD56 BV711	BioLegend	Clone:318335
Anti-human CD69 BUV395	BD	Clone:FN50
Anti-human CD90 PE-Cy5	BD	Clone:5E10
Anti-human HLA-DR PE	ThermoFisher	Clone:LN3
Anti-human CD154 PE-Cy5	BioLegend	Clone:24-31
Anti-human CD197 (CCR7) Pacific Blue	BioLegend	Clone:G043H7
Anti-human CD223 (LAG3) BV711	BioLegend	Clone:11C3C65
Anti-human CD235 APC	BD	Clone:HIR2
Anti-human CD274 (PD-L1) BV785	BioLegend	Clone:29E.2A3

Anti-human CD279 (PD1) APC	BioLegend	Clone:EH12.2H7
Anti-human CD366 (TIM3) BV605	BioLegend	Clone:F38-2f2
Bacterial and Virus Strains		
MCMV-Δm157 (MCMV)	Hirche *et al.*, 2017	N/A
Biological Samples		
Human Healthy Bone Marrow Aspirates	Heidelberg University Hospital	N/A
Human Peripheral Blood	University Hospital Mannheim	N/A
Human AML Bone Marrow Aspirates	AML-SG and SAL biorepositories	N/A
Chemicals, Peptides, and Recombinant Proteins		
pI:C	Invivogen	Cat#tlrl-pic
LPS	ThermoFisher	Cat#00-4976-03
IFNα	Miltenyi	Cat#130-093-131
Ovalbumin	Invivogen	Cat#vac-stova
DQ Ovalbumin	Invitrogen	Cat#D12053
Ovalbumin 323-339 peptide	Invivogen	Cat#vac-isq
Ovalbumin 257-264 peptide	Invivogen	Cat#vac-sin
MOG peptide	Genemed Sythesis	Cat#MOG3555-P2-1
Eα peptide (52-68)	Mimotopes	Cat#68827-005
ACK Buffer	Lonza	Cat#10-548E
Sodium pyruvate	Gibco	Cat#11360039
L-Glutamine	Gibco	Cat#25030081
L-arginine	Sigma	Cat#A5006-100G
L-asparagine	Sigma	Cat#A0884-100G
Penicillin/Streptomycin	Sigma	Cat#P4458-100ml
Folic acid	Sigma	Cat#F7876-10G
MEM non-essential amino acids	ThermoFisher	Cat#11140050
MEM vitamin solution	ThermoFisher	Cat#11120052
β-mercaptoethanol	Sigma	Cat# M3148
Cell Trace Violet	ThermoFisher	Cat#C34557
Dynabeads Mouse T-Activator	ThermoFisher	Cat#11452D
CytoStim	Miltenyi	Cat#130-092-172
PepMix CEFX Ultra SuperStim MHC-II Subset Pool	JPT	Cat#PM-CEFX-3
Mouse TPO	PreproTech	Cat#315-14
Mouse SCF	PreproTech	Cat#250-03
CNBr-activated Sepharose	GE Healthcare	Cat#17-0430-01
Trifluoroacetic acid	Merck	Cat#108262
DNAseI	Roche	Cat#4716728001
2′,7′-Dichlorofluorescin diacetate	Sigma	Cat#D6883-50MG
DAPI	ThermoFisher	Cat#D1306
Sunflower oil	Sigma	S5007-250ML
Tamoxifen	Sigma	T5648-1G
RNAsin+	Promega	N2611
Triton X-100	Sigma	9002-93-1
Smart-seq2 Oligo-dT primer	Sigma	N/A
dNTP mix	NEB	N0447S
ERCC spike-in mix	Ambion	4456740
5x SMART FS buffer	Takara	N/A

DTT	Takara	N/A
SmartScribe	Takara	639538
Smart-seq2 TSO	Exiqon	N/A
Smart-seq2 ISPCR primer	Sigma	N/A
Ctrl IgG2b	ThermoFisher	Clone:eB149/10H5
Anti-Biotin Streptavidin PE	BioLegend	Clone:B123088
Critical Commercial Assays		
Dynabeads Untouched Mouse CD4 Cells Kit	Invitrogen	Cat#11416D
Cell Stimulation Cocktail (plus protein transport inhibitors)	eBioscience	Cat#00-4975-93
Fixation/Permeabilization Solution Kit	BD	Cat#554714
Arcturus PicoPure RNA Isolation Kit	Invitrogen	Cat#KIT0204
SuperScript VILO cDNA synthesis Kit	Invitrogen	Cat#11754050
PowerUP SybrGreen Mastermix	ThermoFisher	Cat#A25741
RNA 6000 Pico Kit	Agilent	Cat#5067-1513
SMARTer Ultra Low Input RNA Kit	Takara	Cat# 634940
NEBNext ChIP-seq Library Prep Kit for Illumina	NEB	Cat# E6240
Qubit™ dsDNA HS Assay Kit	Invitrogen	Cat# Q32851
SureSelect HS XT Target Enrichment System v6	Agilent	N/A
KAPA HiFi HS Mastermix	Merck	
Experimental Models: Mice		
BALB/c	Harlan / Jackson / Taconic	JAX:000651
C57BL/6J	Harlan/Taconic/Jackson Laboratory	JAX:000664
B6.SJL-Ptprca Pepcb/BoyJ	Harlan/Taconic/Jackson Laboratory	JAX:002014
NOD.Cg-PrkdcscidIL2rgtmWjl/SzJ	Jackson	JAX:005557
C57BL/6-Tg(CAG-OVA)916Jen/J	Jackson	JAX:005145
C57BL/6-Tg(Tcra2D2,Tcrb2D2)1Kuch/J	Jackson	JAX:006912
B6.Cg-Tg(TcraTcrb)425Cbn/J	Jackson	JAX:004194
C57BL/6-Tg(TcraTcrb)1100Mjb/J	Jackson	JAX:003831
B6.129S2-Il10rbtm1Agt/J	Jackson	JAX:005027
B6.129S(Cg)-Stat1tm1Dlv/J	Durbin *et al.*, 1996	JAX:012606
BALB/c x C57BL/6J	N/A	N/A
B6-Tg(Tal1-cre)42-056Jrg H2-Ab1tm1Koni Gt(ROSA)26Sortm1(EYFP)Cos/Atp	N/A	N/A
H2-Ab1tm1Koni Gt(ROSA)26Sortm1(EYFP)Cos/Atp	N/A	N/A
Experimental Models: Cell Lines		
CTV-1	Leibniz Institute DSMZ	ACC 40
GDM-1	Leibniz Institute DSMZ	ACC 87
HL-60	Cell Lines Service (CLS)	300209
Kasumi-1	Leibniz Institute DSMZ	ACC 220
Kasumi-3	Leibniz Institute DSMZ	16469
Kasumi-6	Leibniz Institute DSMZ	15974
KG-1	Leibniz Institute DSMZ	ACC 14
KG-1a	Leibniz Institute DSMZ	ACC 421
ME-1	Leibniz Institute DSMZ	ACC 537
ML-1	Leibniz Institute DSMZ	ACC 464
ML-2	Leibniz Institute DSMZ	ACC 15

MOLM-14	Leibniz Institute DSMZ	ACC 777
MONO-MAC-6	Leibniz Institute DSMZ	ACC 124
MV4-11	American Type Culture Collection (ATCC)	ATCC-CRL-9591
NB-4	Leibniz Institute DSMZ	ACC 207
OCI-AML2	Leibniz Institute DSMZ	ACC 99
OCI-AML3	Leibniz Institute DSMZ	ACC 582
OCI-M1	Leibniz Institute DSMZ	ACC 529
PL-21	Leibniz Institute DSMZ	ACC 536
SET-2	Leibniz Institute DSMZ	ACC 608
SKM-1	Leibniz Institute DSMZ	ACC 547
THP-1	Leibniz Institute DSMZ	ACC 16
U-937	Leibniz Institute DSMZ	ACC 5
YNH-1	Leibniz Institute DSMZ	ACC 692
Oligonucleotides		
Mouse primers for qPCR, see Table S1		
Human primers for qPCR, see Table S2		
Software and Algorithms		
Quant StudioTM Real-Time PCR Software v1.3	Applied Biosystems	
FACSDIVA v8.0	BD	
Flowjo v10	TreeStar	
Proteome Discoverer v1.3	ThermoFisher	
Sequest search engine	ThermoFisher	
nSolver Analysis Software	Nanostring	
cluster v2.1.0	Maechler *et al.*, 2019	
NbClust v3.0	Charrad *et al.*, 2014	
ComplexHeatmap v.2.0.0	Gu, Eils and Schlesner, 2016	
DESeq2	Love, Huber and Anders, 2014	
ClusterProfiler	Yu *et al.*, 2012	
GraphPad Prism v8	GraphPad Software	

RESOURCE AVAILABILITY

Lead Contact

Further information and requests for resources and reagents should be directed to and will be fulfilled by the Lead Contact, Simon Haas (simon.haas@bih-charite.de).

Materials Availability

This study did not generate new unique reagents.

Data and Code Availability

Data are available from the corresponding author upon request.

EXPERIMENTAL MODEL AND SUBJECT DETAILS

Mice

All animal experiments were approved by the Animal Care and Use Committees of the German Regierungspräsidium Karlsruhe für Tierschutz und Arzneimittelüberwachung (Karlsruhe, Germany), the Harvard Medical Area Standing Committee on Animals, the Brigham and Women's Hospital Institutional Animal Care and Use Committee (Boston, USA) or the Institutional Animal Care and Use Committees (IACUC) of the Dana-Farber Cancer Institute (Boston, USA). All mice were maintained in individually ventilated cages under SPF conditions in the animal facility of the DKFZ (Heidelberg, Germany), the Hale Building for Transformative Medicine of the Brigham and Women's Hospital (Boston, USA) or Dana-Farber Cancer Institute (Boston, USA). Wild type mice (BALB/c, C57BL/6J (CD45.2) and B6.SJL-Ptprca Pepcb/BoyJ (CD45.1)) were purchased from Harlan Laboratories, Taconic or the Jackson Laboratories. NOD.Cg-PrkdcscidIL2rgtmWjl/SzJ (NSG), C57BL/6-Tg(CAG-OVA)916Jen/J (CAG-OVA), C57BL/6-Tg(Tcra2D2,Tcrb2D2)1Kuch/J (2D2) and B6.Cg-Tg(TcraTcrb)425Cbn/J (OT-II) mice were purchased from the Jackson Laboratories. B6.129S(Cg)-Stat1tm1Dlv/J (*Stat1*$^{-/-}$) and B6.129S2-Il10rbtm1Agt/J (*Il10rb*$^{-/-}$) have been described before (Durbin *et al.*, 1996; Spencer *et al.*, 1998). B6.129S2-Il10rbtm1Agt/J mice were kindly provided by Dr. Laura Llaó-Cid. C57BL/6-FLT3wt/ITD/Mx1-Cre mice were kindly provided by the group of Prof. Dr. Carsten Müller Tidow. C57BL/6-Tg(TcraTcrb)1100Mjb/J (OT-I) mice were kindly provided by Stephanie Lindner from the group of Prof. Dr. Rienk Offringa. BALB/cxC57BL/6J F1 and B6-Tg(Tal1-cre)42-056Jrg H2-Ab1tm1Koni Gt(ROSA)26Sortm1(EYFP)Cos/Atp (SclCreERT2 x MHC-II-flox x Rosa26-EYFP-flox) mice were generated in house.
To induce inflammatory conditions, mice were injected intraperitoneally with a single dose of 5 mg/kg pI:C (Invivogen), 0.25 mg/kg LPS (ThermoFisher), 500U/g IFNα (Miltenyi) and MCMV (Hirche *et al.*, 2017). For administration of ovalbumin, a single dose of 500mg/kg of full ovalbumin protein (Invivogen), 500mg/kg of DQ-OVA (Invitrogen), or 12.5mg/kg of ovalbumin 323-339 peptide (Invivogen) was administered. For knock-out induction, 100mg/kg of tamoxifen were resuspended in sunflower oil with ethanol (10%) and injected intraperitoneally once a day for five consecutive days.

Human samples

Peripheral blood and bone marrow samples from healthy donors were obtained from the University Hospital Mannheim and Heidelberg University Hospital after informed written consent. Mononuclear cells were isolated by density gradient centrifugation and stored in liquid nitrogen until further use. All experiments involving human samples were conducted in compliance with the Declaration of Helsinki and approved by and in accordance with regulations and guidelines by the ethics committee of the medical faculty of the University of Heidelberg.

METHOD DETAILS

Preparation of mouse bone marrow, spleen and lymph nodes

Mouse bone marrow was prepared by crushing femur, tibia, humerus, ilium, sternum and columna vertebralis in PBS (Sigma) supplemented with 2% heat-inactivated FCS (Gibco). Subsequently, cells were filtered through 40µm cell strainers (Falcon) and erythrocyte lysis was performed for 5 min using ACK buffer (Lonza), followed by washing and centrifugation for 5 min at 250 x g. For isolation of HSPCs, cells were incubated in PBS 2% FCS for 15 minutes

with antibodies against the lineage markers CD11b (M1/70), Gr-1 (RB6.8C5), CD4 (GK1.5), CD8a (53.6.7), Ter119 (Ter119) and B220 (RA3-6B2) at 4°C. Subsequently, cells were washed and incubated for 15 minutes with pre-washed anti-rat IgG-coated Dynabeads 4,5µm magnetic polystyrene beads (Invitrogen) in the ratio of 1mL of beads /mouse. Cells expressing lineage markers were depleted using a separation magnet (Invitrogen), followed by staining the remaining lineage-negative cells described below.
Spleen and lymph nodes (inguinal, axial, submandibular, mesenteric) were dissected and homogenized through a 40µm filter into PBS 2% FCS using the plunger of a syringe. Erythrocyte lysis was performed for 5 min using ACK buffer (Lonza). For $CD4^+$ T cell sorts, the Dynabeads Untouched Mouse CD4 Cells Kit (Invitrogen) was used according to the manufacturer's instructions. Enriched cells were stained and isolated by FACS sorting as described below.

Flow cytometry staining, acquisition and FACS sorting

For flow cytometric analyses and FACS sorts, lineage-depleted, $CD4^+$ T cell enriched or unfractionated cells were stained in PBS 2% FCS for 20 min with corresponding antibodies and washed. For Y-Ae antibody conjugated with biotin, cells were washed and incubated for another 20 minutes with Streptavidin-PE (ThermoFisher). For intracellular cytokine staining, cells were stimulated for 4h at 37°C with the Cell Stimulation Cocktail (plus protein transport inhibitors) (eBioscience). After surface staining, cells were fixed, permeabilized and stained using the BD Fixation/Permeabilization Solution Kit (BD Biosciences) according to manufacturer's instructions. Finally, cells were filtered through a 35-40µM filter and acquired by a flow cytometer (LSR II or LSRFortessa, Becton Dickinson) or cell sorter (FACSAria II or FACSAria Fusion, Becton Dickinson) for analysis or sort, respectively. Common gating strategies used in this study to define populations are depicted in Figures S9 and S10.

Quantitative Polymerase Chain Reaction (qPCR)

For qPCR analyses, cells were directly sorted into RNA lysis buffer (Arcturus PicoPure RNA Isolation Kit (Invitrogen), incubated for 30 min at 42°C and processed for cDNA synthesis using SuperScript VILO cDNA synthesis kit (Invitrogen) according to manufacturer's instructions. The newly synthesized cDNA was diluted 1:10 in RNase free H_2O and 6 µL were mixed in technical triplicates in 384-well plates with 0.5 µl of forward and reverse primer (10 µM) (Table S1 and S2) and 7 µl PowerUP SybrGreen Mastermix (ThermoFisher). Program: 50°C for 2 minutes, 95°C for 10 minutes and 40 cycles of 95°C for 15 seconds, 60°C 1 minute. Primers were designed to be intron spanning whenever possible using the Universal ProbeLibrary Assay Design Center (Roche) and purchased from Sigma Aldrich. Experiments were performed on the ViiA7 System (ThermoFisher) and analysis of gene amplification curves was performed using the Quant StudioTM Real-Time PCR Software v1.3 (Applied Biosystems). RNA expression was normalized to the housekeepers *Gapdh/Actb* for murine and *B2M/ACTB* for human gene expression analysis. Relative expression levels are depicted in $2^{-\Delta Ct}$ values, ΔCt = (geoMean Housekeeper Ct) - (gene of interest Ct).

Murine *ex vivo* cultures

Cells were cultured at 37°C and 5% CO_2 in U-bottom plates in a total volume of 200µL of Dulbecco's Modified Eagle's Medium GlutaMAX (DMEM GlutaMAX, Gibco) supplemented with 10% heat-inactivated Fetal Calf Serum (FCS, Gibco), sodium pyruvate (1.5mM, Gibco), L-

glutamine (2mM, Gibco), L-arginine (1x, Sigma), L-asparagine (1x, Sigma), penicillin/streptomycin (100 U/mL, Sigma), folic acid (14µM, Sigma), MEM non-essential amino acids (1x, ThermoFisher), MEM vitamin solution (1x, ThermoFisher) and β-mercaptoethanol (57.2µM, Sigma). Cells were sorted and, when mentioned, labelled with cell trace violet (ThermoFisher) according to manufacturer's instructions. $5x10^4$ naïve $CD4^+$ T cells were cultured with $2x10^4$ HSPCs, DCs or $CD8^+$ T cells, unless stated otherwise. When stated, ovalbumin peptides (323-339 or 257-264) (both 25µg/mL, Invivogen), full ovalbumin protein (10 mg/mL, Invivogen), DQ-OVA (100µg/mL, Invitrogen), MOG peptide (50µg/mL, Genemed Sythesis), Eα peptide (52-68) (100µg/mL, Mimotopes), LPS (100 ng/mL, ThermoFisher), αMHC-II blocking antibody (10µg/mL, M5/114.15.2, BioXCell) or a control IgG2b antibody (10µg/mL, eB149/10H5, ThermoFisher) were added to the cultures. For transwell experiments, cells were plated as described with additional $2x10^4$ HSPCs plated on 96-well plate inserts with polyester membrane and 1 µm pore size (Corning). For resting of T cells, culture medium was replaced by fresh culture medium in the absence of ovalbumin peptide, followed by culturing for two days. Re-stimulation was performed by addition of Dynabeads Mouse T-Activator (ThermoFisher) according to manufacturer's instructions.

Human *ex vivo* cultures

Human cells were cultured under the same conditions as murine cells. For T cell interaction assays, $5x10^4$ naïve $CD4^+$ T cells were cultured with $5x10^3$ antigen presenting cells (either DCs, $CD34^+$ HSPCs or additional T cells) from an unrelated donor in the presence or absence of CytoStim (Miltenyi) according to manufacturer's instructions. All analyses were performed after three days of co-culture.

Transplantation experiments

For mouse stem cell transplantation experiments, HSPCs were transplanted intravenously into lethally irradiated (2x500rad) recipient mice together with 10^5 rescue bone marrow cells. When mentioned, 10^6 naïve OT-II mice were co-transplanted at the stated time points. Mice were bled periodically and cells were stained as described above for assessment of engraftment. After 4 months, mice were sacrificed, analyzed for engraftment and 10^6 bone marrow cells were intravenously transplanted into secondary lethally irradiated recipients. For xenotransplantation assays, indicated fractions were sorted from human bone marrow aspirates, and 10^5 sorted cells were transplanted intrafemorally into sublethal irradiated (175x1rad) NSG mice. Engraftment of human cells was measured by flow cytometry.

Adoptive co-transfer of OVA-loaded HSCs and antigen-specific T cells

$1.5x10^5$ BM OT-II $CD4^+$ T cells were sorted and intravenously transferred into Ly5.1 mice. LSK cells were isolated as described above and cultured for 12 hours in presence or absence of ovalbumin peptide (50µg/mL) in culture medium supplemented with TPO (50 ng/mL, PreproTech) and SCF (50 ng/mL, PreproTech) at 37°C, 5% CO_2 levels. Subsequently, cells were washed and ($1x10^5$ cells per mouse) adoptively transferred into the recipient mice from above. After three days, mice were sacrificed and the BM was isolated for flow cytometric analysis of HSPC-derived cells.

MLL-AF9 experiments

LSK or GMP cells were sorted and transduced with an MLL-AF9 construct and transplanted into C57BL/6J mice (Taconic) as previously described (Krivtsov *et al.*, 2006, 2013). One month post-transplant, mice were sacrificed and leukemic GFP^+ cells were sorted and co-cultured with naïve OT-II T cells as described above. Alternatively, 10^6 naïve OT-II T cells were co-transplanted when stated and the disease growth in blood was measured weekly. Bone marrow and spleen of mice were analyzed at the endpoint.

Immunopeptidomics

Isolation of MHC ligands

$2.5x10^7$-$5x10^7$ splenocytes ($CD3^-$), T cells ($CD3^+$) or HSPCs (Lineage-cKit+) were sorted and snap frozen. The MHC class II molecules were isolated using standard immunoaffinity purification (Falk *et al.*, 1991; Kowalewski and Stevanović, 2013). In brief, snap-frozen primary samples were lysed in 10 mM CHAPS/PBS (AppliChem) with 1× protease inhibitor (Roche). For the immunoprecipitation of MHC class II–peptide complexes the monoclonal antibody M5/114.15.2 (eBioscience) covalently linked to CNBr-activated Sepharose were used (GE Healthcare). MHC–peptide complexes were eluted by repeated addition of 0.2% TFA (trifluoroacetic acid, Merck). Eluted MHC ligands were purified by ultrafiltration using centrifugal filter units (Amicon). Peptides were desalted using ZipTip C18 pipette tips (Millipore), eluted in 35 µl 80% acetonitrile (Merck)/0.2% TFA, vacuum-centrifuged and resuspended in 25 µl of 1% acetonitrile/0.05% TFA and samples stored at − 20 °C until LC–MS/MS analysis.

Analysis of MHC ligands by LC–MS/MS

Isolated peptides were separated by reversed-phase liquid chromatography (nano-UHPLC, UltiMate 3000 RSLCnano; ThermoFisher) and analyzed in an online-coupled Orbitrap Fusion Lumos mass spectrometer (ThermoFisher). Samples were analyzed in three technical replicates and sample shares of 33% trapped on a 75 µm × 2 cm trapping column (Acclaim PepMap RSLC; Thermo Fisher) at 4 µl/min for 5.75 min. Peptide separation was performed at 50 °C and a flow rate of 175 nl/min on a 50 µm × 25 cm separation column (Acclaim PepMap RSLC; Thermo Fisher) applying a gradient ranging from 2.4 to 32.0% of acetonitrile over the course of 90 min. Samples were analyzed on the Orbitrap Fusion Lumos implementing a top-speed CID method with survey scans at 120k resolution and fragment detection in the Orbitrap (OTMS2) at 60 k resolution. A mass range of 300–1500 *m/z* was analyzed with charge states ≥ 2 selected for fragmentation.

Database search and spectral annotation

LC-MS/MS results were processed using Proteome Discoverer (v.1.3; ThermoFisher) to perform database search using the Sequest search engine (ThermoFisher) and the murine proteome as reference database annotated by the UniProtKB/Swiss-Prot (http://www.uniprot.org), status February 2014 containing 20,270 ORFs. The search combined data of three technical replicates, was not restricted by enzymatic specificity and oxidation of methionine residues was allowed as dynamic modification. Precursor mass tolerance was set to 5 ppm, and fragment mass tolerance to 0.02 Da. False discovery rate was estimated using the Percolator node (Käll *et al.*, 2007) and was limited to 5%. Peptide length was limited to 12–25 AA of length.

NanoString and RNA-Seq gene expression analysis

After 3 days of co-culture with $2.5x10^3$ (NanoString) or $2x10^4$ (RNA-Seq) HSPCs or $2x10^4$ DCs, $CD4^+$ T cells were FACS-sorted and lysed in RLT Buffer (Qiagen) with 1% β-mercaptoethanol (Sigma). For NanoString, RNA was hybridized with the PanCancer Mouse Immune Profiling CodeSet provided by NanoString Technologies. The barcodes were counted on an nCounter Digital Analyzer. The obtained raw data was analyzed using the nSolver Analysis Software. For RNA-Seq, the SmartSeq2 protocol was followed (Picelli *et al.*, 2013, 2014) and sequenced on an Illumina NextSeq 550 (75bp high-output). Differential expression between samples was tested using the R/Bioconductor package DESeq2 (Love, Huber and Anders, 2014). GSEA was run with the R/Bioconductor package clusterProfiler (Yu *et al.*, 2012).

In vitro suppression assay

T_{DCs} and T_{HSCs} were generated by 3 days of culture as described above, rested in the absence of ovalbumin peptide for 2 days and FACS-sorted. Subsequently, 10^5 CTV-labelled naïve bystander $CD4^+$ or $CD8^+$ T cells were cultured with 10^5 $CD19^-CD3^-$ splenocytes and different ratios of *in vitro*-generated T_{HSCs} or T_{DCs}, or freshly purified $CD4^+$ T_{regs} relative to the amount of naïve bystander $CD4^+$ T cells, and anti-CD3 antibody (1 µg/mL,145-2C11, BioXCell). Cells were analyzed by flow cytometry and proliferation of bystander cells was assessed.
Suppression index = (Sample CTV gMFI) / (No T cell activation CTV gMFI)
Proliferation index = Σ ((# of cells in i) / 2^i *i) / (Σ ((# of cells in i) / 2^i)) - (# of cells in i=0))
i = Number of cell divisions, seen by CTV dilution

In vitro $CD8^+$ T cell cytotoxicity assay

$5x10^4$ CTV-labelled naïve OT-I $CD8^+$ T cells were co-cultured with $5x10^4$ naïve OT-II $CD4^+$ T cells and $2x10^4$ $CD19^-CD3^-$ splenocytes or HSPCs in the presence or absence of the MHC-I- and/or MHC-II-restricted OVA peptides. T cells and APCs were analyzed after 3 days via flow cytometry. Cytotoxicity was measured by annexin V positivity in the APCs.

In vitro macrophage polarization assay

T_{DCs} and T_{HSCs} were generated by 3 days of culture as described above, rested in the absence of ovalbumin peptide for 2 days and FACS-sorted. Subsequently, $5x10^4$ freshly sorted T_{DCs} or T_{HSCs} were cultured with 10^5 $CD19^-CD3^-CD11b^+SSC^{low}$ bone marrow monocytes and macrophages and anti-CD3/anti-CD28 activating beads according to manufacturer's instructions. Cells were analyzed after 24 hours by flow cytometry.

In vivo suppression assay

For the *in vivo* suppression assay, T_{DCs} and T_{HSCs} were generated as described above and FACS sorted at day 3 of the co-culture. Subsequently, $1.5x10^5$ cells were adoptively transferred intravenously together with 10^6 CTV-labelled naïve OT-II $CD4^+$ T cells into naive mice. One day post transfer, mice were injected with ovalbumin peptide and LPS as described above, and splenic T cells were analyzed after 3 days via flow cytometry. The proliferation index was calculated as described above.

EuroFlow analysis of diagnostic AML samples

Diagnostic bone marrow aspirates of AML patients were analyzed using the EuroFlow panels (van Dongen *et al.*, 2012) at the University Hospital Heidelberg, Germany. AML blast cells

were gated in FlowJo as $CD45^{+}$ excluding $CD45^{high}SSC^{low}$ healthy lymphoid cells, and geometric mean fluorescence intensities (gMFIs) for all FACS markers were exported. Before z-score scaling the data, values larger than the 95 percentile and smaller than the 5 percentile were considered to be outliers and adjusted to the 95 or 5 percentile, respectively. The data was partitioned into 4 clusters by PAM (partitioning around medoids) clustering using the R package cluster v2.1.0 (Maechler *et al.*, 2019), after determining the best number of clusters using NbClust v3.0 (Charrad *et al.*, 2014). Heatmap visualizations of the data were done using the R/Bioconductor package ComplexHeatmap v.2.0.0 (Gu, Eils and Schlesner, 2016). Stem-, Mono-, and Granulo-indices were calculated by adding the scaled gMFIs of the respective signature for each patient and min-max feature scaling each index between patients: Stem-index = CD34 and CD117, Mono-index = CD14, CD64, CD300e and CD45, Granulo-index = CD35, CD15, CD16 and SSC-A.

Statistical analysis and representation

Flow cytometric analyses were performed in FlowJo (BD). Bioinformatic analyses were performed in R, and visualized or further analyzed in R or GraphPad Prism (v8.4.2, GraphPad Software). The vast majority of ex vivo experiments have been performed multiple times. Most experiments for large-scale gene and protein expression analyses and in vivo experiments, have been performed once. The number of biological replicates per experiment are indicated in the figure legends. Statistical tests used in every figure legend. In short, one- or two-way ANOVA, or Kruskal-Wallis tests were performed as discovery tests wherever necessary. Only when the discovery test was significant, post-hoc two-tailed t-tests or Mann-Whitney tests were performed based on normality of the data. In case of multiple comparisons, p-values were corrected by the Benjamini-Hochberg false discovery rate of 5% and q-values were subsequently used to indicate significance. Significance is depicted as: no significance = ns, $P<0.05$ *, $P<0.01$ **, $P<0.001$ ***, $P<0.0001$ **** according to statistical tests indicated in each figure legend.

Supplemental Information

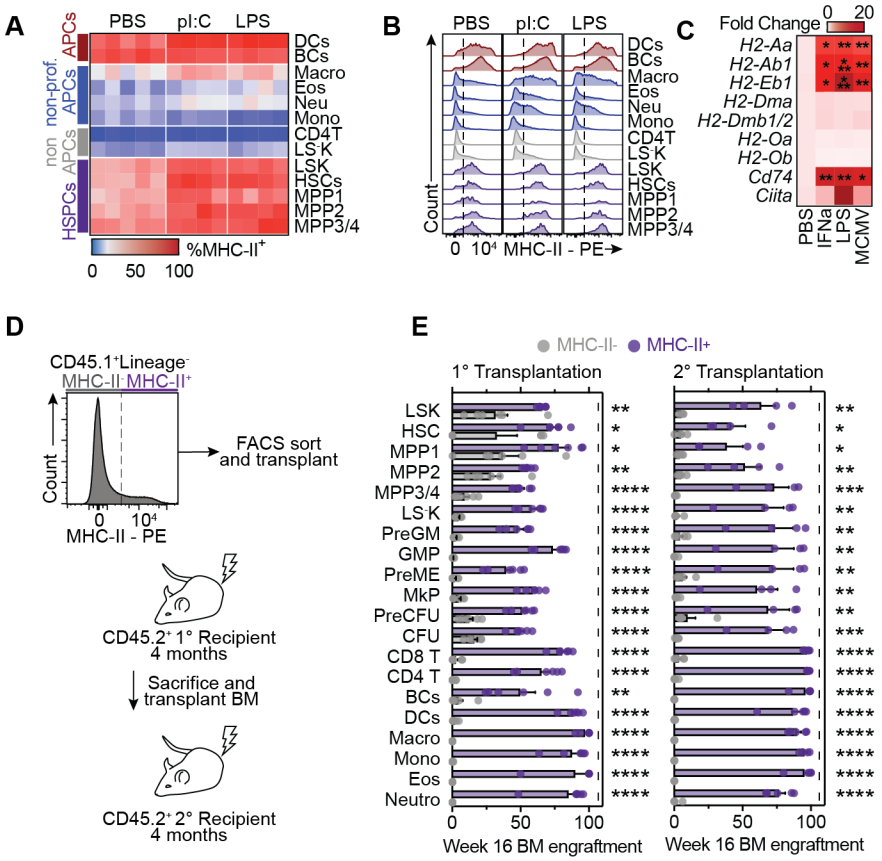

Figure S1. MHC-II expression and regulation in mouse.

Related to Figure 1.

(**A** and **B**) MHC-II surface measurements by flow cytometry of indicated populations at homeostasis or 24 hours post LPS or pI:C treatment. (**A**) Heatmap summarizing MHC-II surface expression, *n*=4-5. (**B**) Representative histograms with dashed lines indicating thresholds for gating.

(**C**) Relative gene expression of MHC-II genes across sorted bone marrow HSCs (Lin^- $cKit^+CD150^+CD48^-$) measured by qPCR. Mice were treated with indicated agents 24 hours prior to the sort. Gene expression is displayed relative to PBS treatment, *n*=3.

(**D**) Experimental design corresponding to Figure 1E and Figure S1E.

(**E**) Bone marrow engraftment levels of transplanted MHC-II bone marrow populations across different mature and progenitor cell types at the endpoint of the primary (left, 4 months post primary) and secondary (right, 4 months post-secondary) transplantations, *n*=4-6.

Individual values are depicted in A means are depicted in C and means and SEM are depicted in all other panels. No significance = ns, P<0.05 *, P<0.01 **, P<0.001 ***, P<0.0001 ****. One-way ANOVA (C and E) was performed as discovery test. If not stated otherwise, unpaired two-tailed t-tests were performed as post-hoc tests. In case of multiple comparisons, p-values were corrected according to Benjamini-Hochberg.

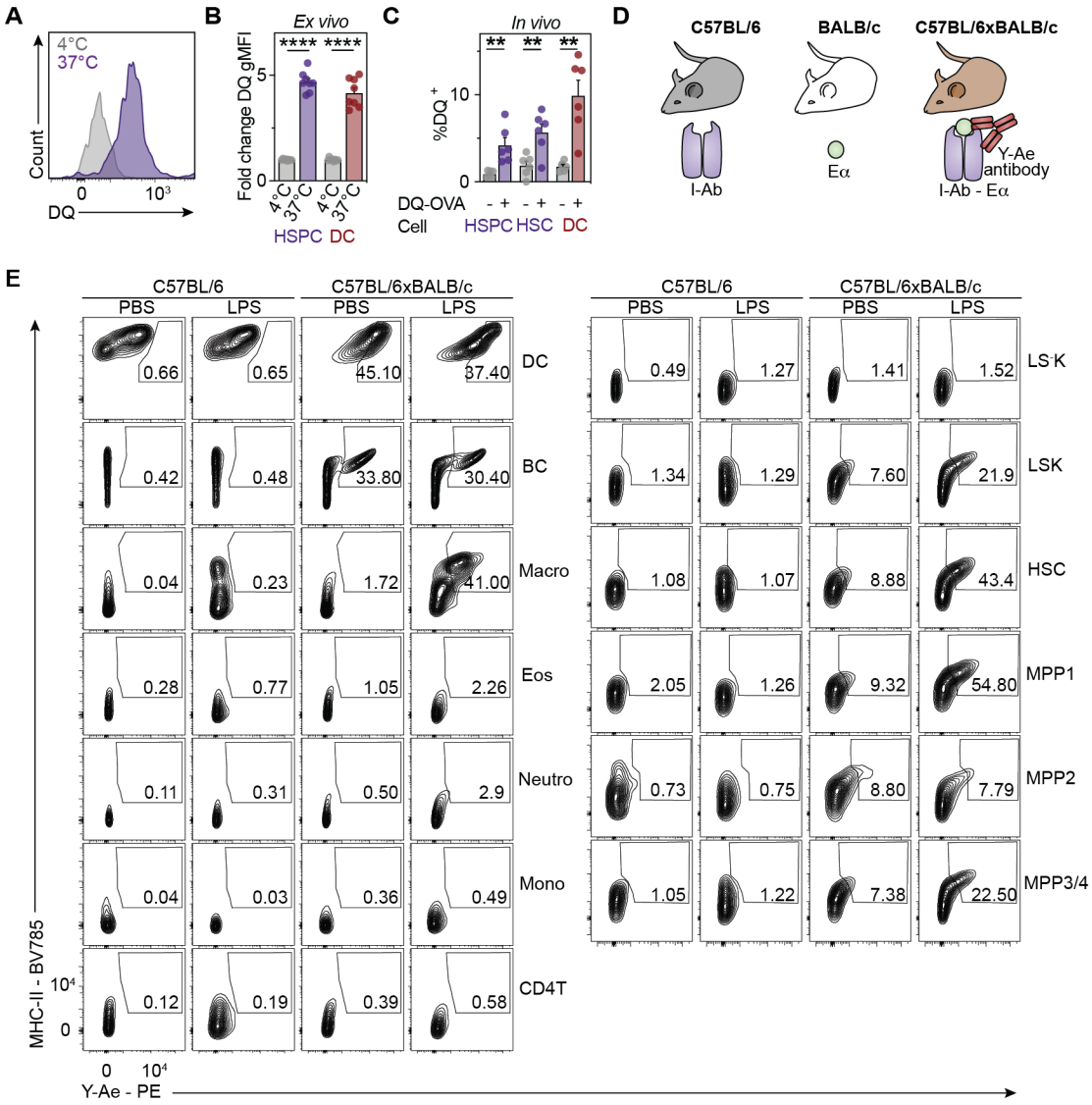

Figure S2. Antigen processing and presentation by HSPCs.

Related to Figure 2.

(**A**) Flow cytometry analyses of HSPCs and DCs *ex vivo* cultured in the presence of DQ-OVA. Cells were cultured for three hours at 4°C or 37°C and analyzed for intake and processing. Representative HSPC plots (**A**) and quantification (**B**) are depicted, *n=8*.

(**C**) Antigen intake and processing *in vivo*. DQ-positive cells were measured 2 hours after DQ-OVA injection, *n=6*.

(**D**) Schematic illustration related Figure 2B, 2C and S2E. The presence of the I-A^{d} haplotype and Eα peptide in each of the used mouse strains and ability of Y-Ae antibody to bind only the combination of both is displayed.

(**E**) Representative FACS plots of *in vivo* antigen presentation assay of Figure 2, B and C. Numbers represent percentages of cells inside the gates. The Y-Ae antibody was used to measure presentation of Eα via MHC-II in C57BL/6xBALB/c mice and control C57BL/6 mice at homeostasis or 24 hours post LPS treatment. Boxes indicate quantified populations.

Means and SEM are depicted. No significance = ns, P<0.05 *, P<0.01 **, P<0.001 ***, P<0.0001 ****. One-way ANOVA (B and C) was performed as discovery test. If not stated otherwise, unpaired two-tailed t-tests were performed as post-hoc tests. In case of multiple comparisons, p-values were corrected according to Benjamini-Hochberg.

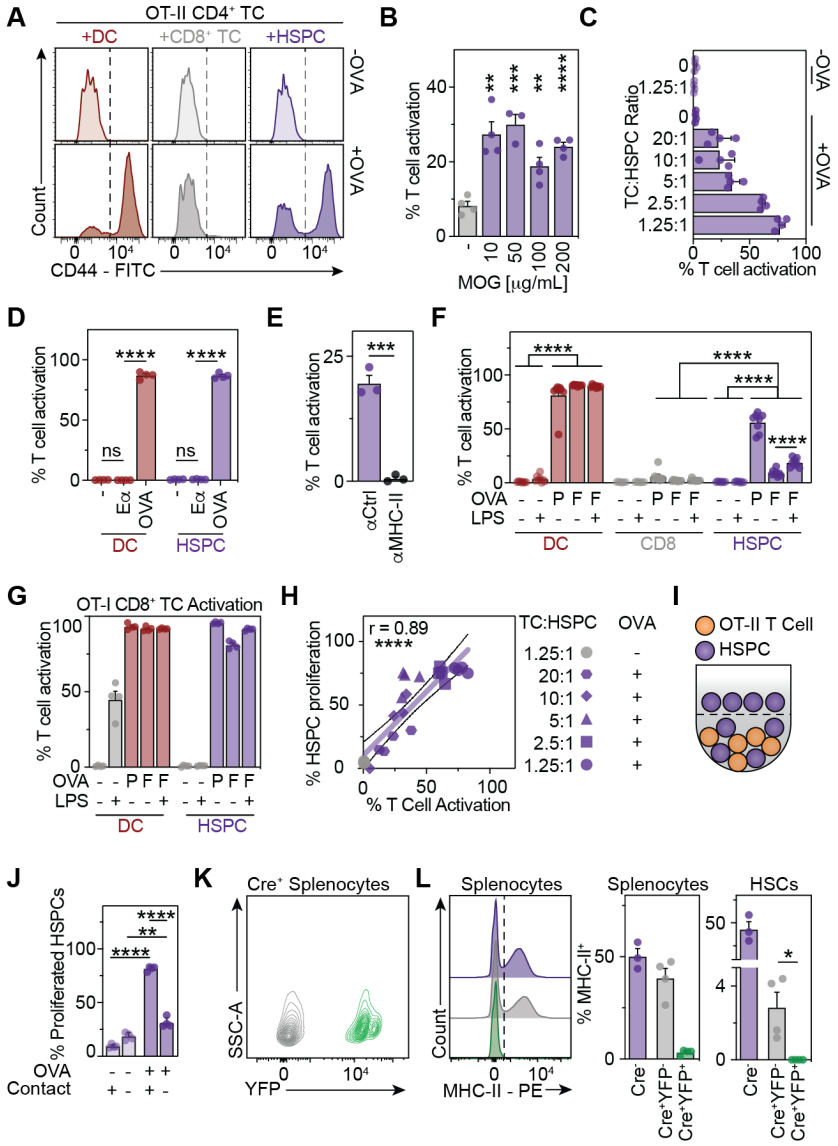

Figure S3. Bidirectional interactions between HSPCs and CD4⁺ T cells.

Related to Figure 3.

Evaluation of antigen presentation capacity by co-cultures of naïve T cells with HSPCs (LSKs) and selected control populations in the presence or absence of MHC-restricted peptides or full proteins after 72 hours of co-culture. MHC-I-restricted OVA peptide and OT-I CD8⁺ T cells were used in (G), MHC-II-restricted MOG and 2D2 CD4⁺ T cells in (B) and MHC-II-restricted OVA peptide and OT-II CD4⁺ T cells in the remaining if not otherwise indicated.

(**A**) Representative histograms of CD44 expression from Figure 3B. Dashed lines indicate segregation between naïve and activated CD4⁺ T cells

(**B**) Evaluation of antigen presentation capacity of 2D2 CD4⁺ T cells with HSPCs (LSKs) in the presence or absence of MOG MHC-II-restricted peptide, *n*=4.

(**C**) Proliferation and activation assay of OT-II CD4⁺ T cells upon co-culture with different numbers of HSPCs. Proliferation was read out CTV labelling dilution and activation by CD44 staining, *n=4*.

(**D**) Activation assay of OT-II CD4⁺ T cells upon co-culture with HSPCs and DCs, in the absence of peptide, in the presence of OT-II-non-specific Eα peptide or in the presence of the OT-II-specific OVA peptide, *n=4*.

(**E**) T cell activation upon co-culture with a MHC-II-blocking antibody or isotype control, *n=3*.

(**F**) Quantification of T cell activation in co-cultures in the absence (-) or presence of OVA peptide (P) or full OVA protein (F) with (+) or without (-) LPS, *n=8*.
(**G**) Quantification of OT-I $CD8^+$ T cell activation in co-cultures in the absence (-) or presence of OVA peptide (P) or full OVA protein (F) with (+) or without (-) LPS, *n=4*.
(**H**) Correlation of T cell activation with HSPC proliferation. Different numbers of HSPCs were co-cultured with naïve OT-II T cells in the presence or absence of OVA for three days. Linear regression with 95% CI, *n=4*.
(**I** and **J**) Contact-dependent assessment of HSPC proliferation. (**I**) Experimental scheme. Co-cultures were performed in a transwell plate with HSPCs in contact with T cells in the lower well and the same amount of HSPCs in the upper insert without contact to OT-II $CD4^+$ T cells.
(**J**) Proliferation of HSPCs was quantified based on CTV dilution, *n*=4.
(**K**) YFP upregulation upon tamoxifen treatment. Representative flow cytometry plot of total spleen from a Cre^+ mouse treated with tamoxifen.
(**L**) MHC-II downregulation upon tamoxifen treatment. Left, representative MHC-II plot of total spleen from a Cre^- mouse (purple), and YFP- (gray) or YFP+ (green) from a Cre^+ mouse, all treated with tamoxifen. Dashed line depicts quantification threshold for MHC-II positivity. Quantification of MHC-II^+ cells in splenocytes from the stated populations (middle) or HSCs from bone marrow (right), *n=3-4*.
Means and SEM are depicted. No significance = ns, P<0.05 *, P<0.01 **, P<0.001 ***, P<0.0001 ****. One- (B, C, D, and L) or two-way ANOVA (F, G and J) were performed as discovery tests. Linear regression analysis was performed in H. If not stated otherwise, unpaired two-tailed t-tests were performed as post-hoc tests. In case of multiple comparisons, p-values were corrected according to Benjamini-Hochberg.

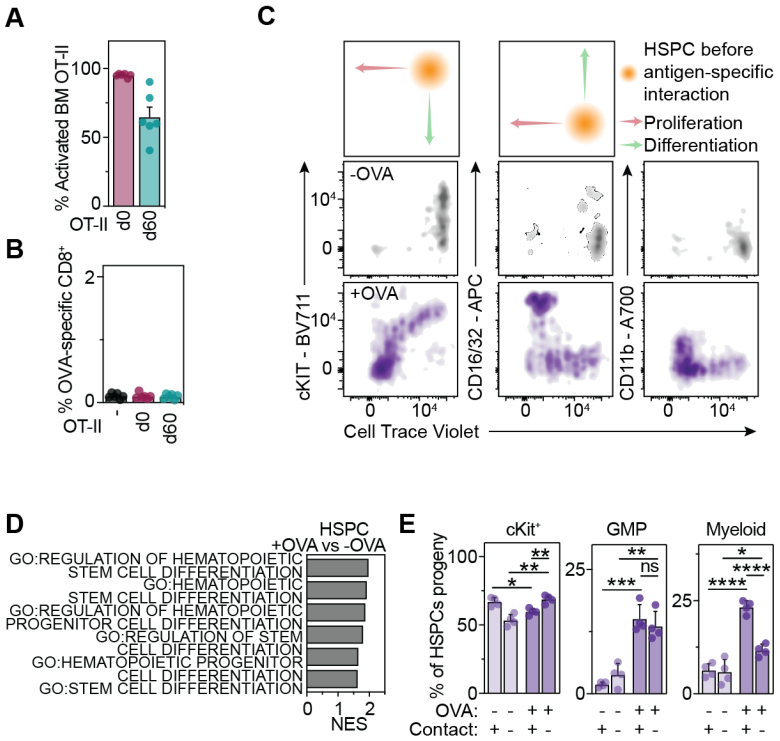

Figure S4. HSPCs differentiate upon antigen-specific interaction with CD4⁺ T cells

Related to Figure 4.

(**A**) Percentage of OT-II T cells with a CD44⁺ antigen-experienced phenotype, *n*=6.

(**B**) Percentage of OVA-specific CD8⁺ T cells in bone marrow after 20 weeks, *n*=6.

(**C**) Differentiation and stemness markers in relation to HSPC proliferation upon CD4⁺ T cell activation. Proliferation of HSPCs was read out by CTV dilution 72 hours post co-culture with OT-II in the absence (middle panels) or presence of OVA (lower panels). Schematic representation of HSPCs before antigen-specific interactions and its consequences are illustrated in the upper panels. Representative FACS plots from Figure 4G are depicted.

(**D**) HSC differentiation genes are upregulated upon antigen presentation. Bulk RNA-Seq of HSPCs co-cultured with OT-II T cells for 72 hours in the presence or absence of OVA peptide, *n=3-4*. GSEA was performed in the RNA-Seq data, and normalized enrichment score (NES) of HSC-related gene sets are represented.

(**E**) Contact-dependent assessment of HSPC proliferation and differentiation. Co-cultures were performed in a transwell plate with HSPCs in contact with T cells in the lower well and the same amount of HSPCs in the upper insert without contact to OT-II CD4⁺ T cells. Differentiation was quantified as in Figure 4 *n*=4.

Means and SEM are depicted otherwise. No significance = ns, P<0.05 *, P<0.01 **, P<0.001 ***, P<0.0001 ****. One- (B) or two-way ANOVA (E) were performed as discovery tests. Unpaired two-tailed t-tests were performed as post-hoc tests and p-values were corrected according to Benjamini-Hochberg.

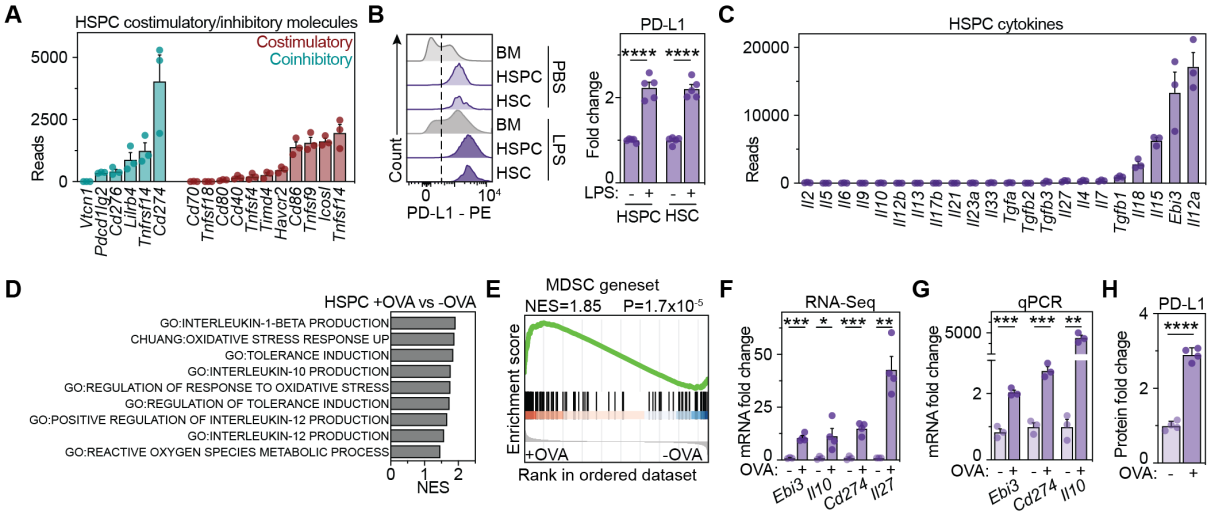

Figure S5. Immunogenic characterization of HSPCs before and after T cell activation.
Related to Figure 5.

(**A**) Reads of genes encoding the main T cell costimulatory/inhibitory molecules in mouse HSPCs taken from genome-wide RNA-Seq data (Klimmeck *et al.*, 2014), *n*=3.

(**B**) PD-L1 surface measurements by flow cytometry of total bone marrow (BM), HSPCs and HSCs at homeostasis or 24 hours post LPS treatment. Representative histograms (left) and quantification of fluorescence intensity relative to PBS of each population (right), *n*=5. Dashed lines indicate thresholds for positivity.

(**C**) Reads of genes encoding the main T cell instructing/polarizing cytokines in mouse HSPCs inferred from genome-wide RNA-Seq data (Klimmeck *et al.*, 2014), *n*=3.

(**D**) HSC differentiation genes are upregulated upon antigen presentation. Bulk RNA-Seq of HSPCs co-cultured with OT-II T cells for 72 hours in the presence or absence of OVA peptide, *n=3-4*. GSEA was performed in the RNA-Seq data, and normalized enrichment score (NES) of HSC-related gene sets are represented.

(**D-H**) Tolerogenic genes are upregulated upon antigen presentation in HSPCs. HSPCs were co-cultured, as previously, with OT-II T cells for 72 hours in the presence or absence of OVA peptide, *n=3-4*.

(**D**) GSEA was performed in the RNA-Seq data, and normalized enrichment score (NES) of tolerance-related gene sets are represented.

(**E**) GSEA for a myeloid derived suppressive cell (MDSC) comprehensive gene set (Alshetaiwi *et al.*, 2020).

(**F** and **G**) Individual and crucial tolerogenic genes from RNA-Seq (F) are plotted and reconfirmed by qPCR (G) of OVA-incubated HSPCs relative to -OVA condition, *n=3-4*.

(**H**) PD-L1 surface expression on HSPCs of OVA-incubated HSPCs relative to -OVA condition, *n=4*.

Means and SEM are depicted. No significance = ns, P<0.05 *, P<0.01 **, P<0.001 ***, P<0.0001 ****. One-way ANOVA was performed in B, F and G as discovery test, followed by unpaired two-tailed t-tests as post-hoc tests. In case of multiple comparisons, p-values were corrected according to Benjamini-Hochberg.

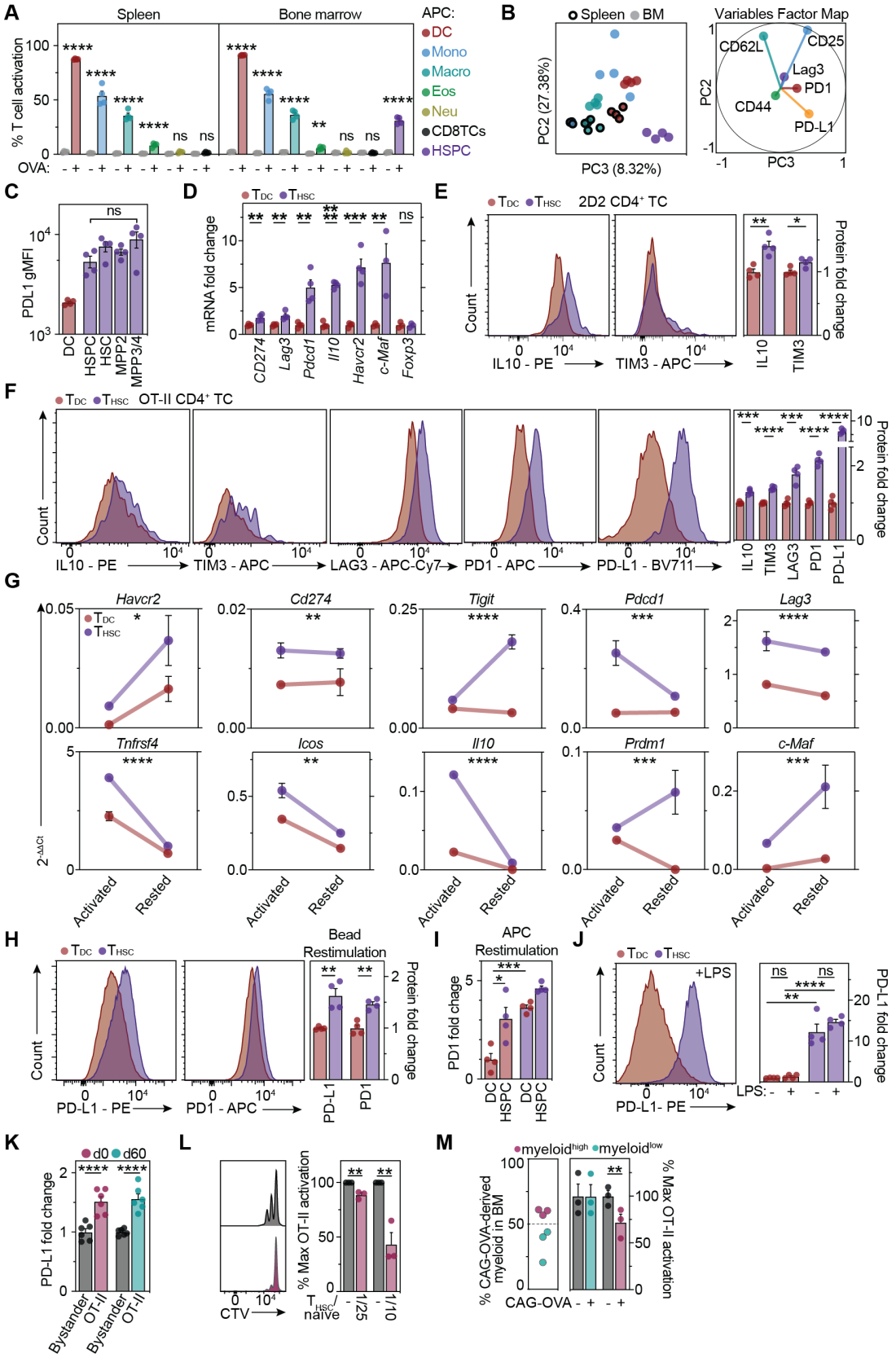

Figure S6. Immunophenotypic characterization of T_{HSCs}.

Related to Figure 5.

(**A** and **B**) Naïve OT-II T cells were cultured with the same number of different APCs from spleen or bone marrow in the presence or absence of OVA. (**A**) Percentage of T cell activation

was quantified as previously and is represented for all the different APCs tested. (**B**) Principal component analysis (PCA) was performed on activated T cells (left), considering the expression of several T cell activation surface markers represented in the variables factor map (right).

(**C**) $CD4^+$ cells activated by highly purified HSCs and MPPs upregulate the immunoregulatory molecule PD-L1. Fluorescence intensity measured by flow cytometry of PD-L1 surface expression on $CD4^+$ T cells activated by DCs and different subsets of HSPCs.

(**D**) T_{HSC} gene expression. T_{HSCs} and T_{DCs} were generated as previously, and qPCRs were performed for the depicted genes. Gene expression is presented relative to housekeeping genes and T_{DCs}, *n*=4.

(**E** and **F**) Flow cytometric analyses of T_{HSCs} and T_{DCs} from 2D2 (**E**) or OT-II (**F**) T cells. Representative plots (left panels) and quantification relative to T_{DCs} (right panel), *n*=4.

(**G**) qPCR analyses of T_{HSCs} and T_{DCs}. T_{HSCs} and T_{DCs} were generated as previously and rested for 2 days without peptide. *n*=4.

(**H**) The immune suppressive phenotype of T_{HSCs} is maintained upon antigen-unspecific re-activation of T_{HSCs}. T_{HSCs} and T_{DCs} were generated as previously, followed by 2 days of rest without peptide and 2 days of culture with αCD3/αCD28 beads. PD-L1 and PD1 flow cytometry representative histograms are depicted (left). Protein expression is presented relative to T_{DCs} (right), *n*=4.

(**I**) The immunosuppressive phenotype of T_{HSCs} is maintained upon antigen-specific re-activation of T_{HSCs} and induced in HSPC-activated T_{DCs}. T_{HSCs} and T_{DCs} were generated as previously, followed by 2 days of rest without peptide and 2 days of culture with DCs or HSPCs. T_{DCs} and T_{HSCs} are displayed with red or purple bars, respectively. PD1 expression is presented relative to DC-restimulated T_{DCs}, *n*=4.

(**J**) The immune suppressive phenotype of T_{HSCs} is maintained upon inflammation. T_{HSCs} and T_{DCs} were generated as previously in the presence or absence of LPS. PD-L1 flow cytometry representative histograms are depicted (left), and quantified (right), *n*=4.

(**K-M**) Sustained *in vivo* bone marrow antigen-specific HSPC-T cell interactions trigger an immune privileged niche. See Figure 4A for detailed experimental setup.

(**K**) PD-L1 flow cytometry analyses of OT-II and bystander $CD4^+$ T cells in transplanted mice. Surface expression is presented relative to the bystander compartment at the endpoint of the experiment, *n*=4.

(**L**) WT-derived bone marrow cells and OT-II T cells were isolated from the bone marrow of CAG-OVA and WT 50:50 chimeras transplanted mice (see Figure 4A) and cultured with CTV-stained naïve OT-II cells. Three days after, naïve OT-II cell proliferation was measured (left) and quantified (right).

(**M**) WT- and CAG-OVA-derived bone marrow cells a were isolated from the bone marrow of mice as shown in Figure 4A, that promoted CAG-OVA myeloid differentiation with different efficiencies (left) and cultured with CTV-stained naïve OT-II cells. Three days after, naïve OT-II cell proliferation was measured (left) and quantified (right).

Individual values are depicted in B and means and SEM otherwise. No significance = ns, P<0.05 *, P<0.01 **, P<0.001 ***, P<0.0001 ****. One- (A, C, D, E, F, H, K, L, M) or two-way ANOVA (I and J) were performed as discovery tests. Two-way ANOVA is shown in G. Unpaired two-tailed t-tests were performed as post-hoc tests. In case of multiple comparisons, p-values were corrected according to Benjamini-Hochberg.

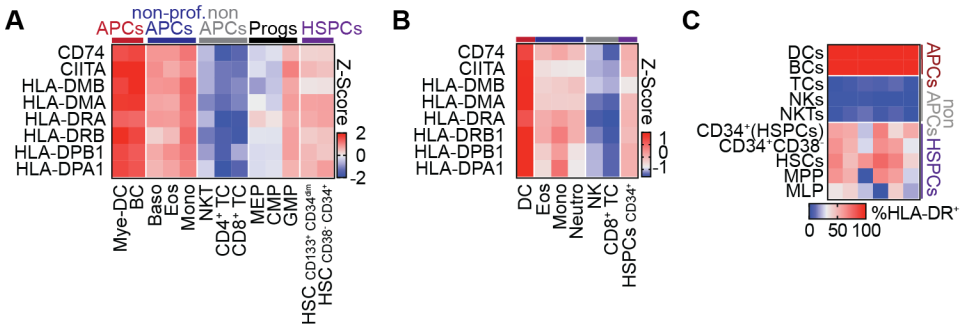

Figure S7. Human HSPCs express the MHC-II machinery.

Related to Figure 6.

(**A** and **B**) MHC-II machinery expression across different human bone marrow populations. z-scores of genes encoding the MHC-II antigen presentation machinery in different human populations, inferred from microarray (Novershtern *et al.*, 2011) (**A**) or RNA-Seq (Hay *et al.*, 2018) (**B**) data.

(**C**) Surface expression of MHC-II in human HSPCs. Heatmap representing HLA-DR (MHC-II) surface measurements by flow cytometry of selected populations from bone marrow aspirates of healthy donors, *n=6*.

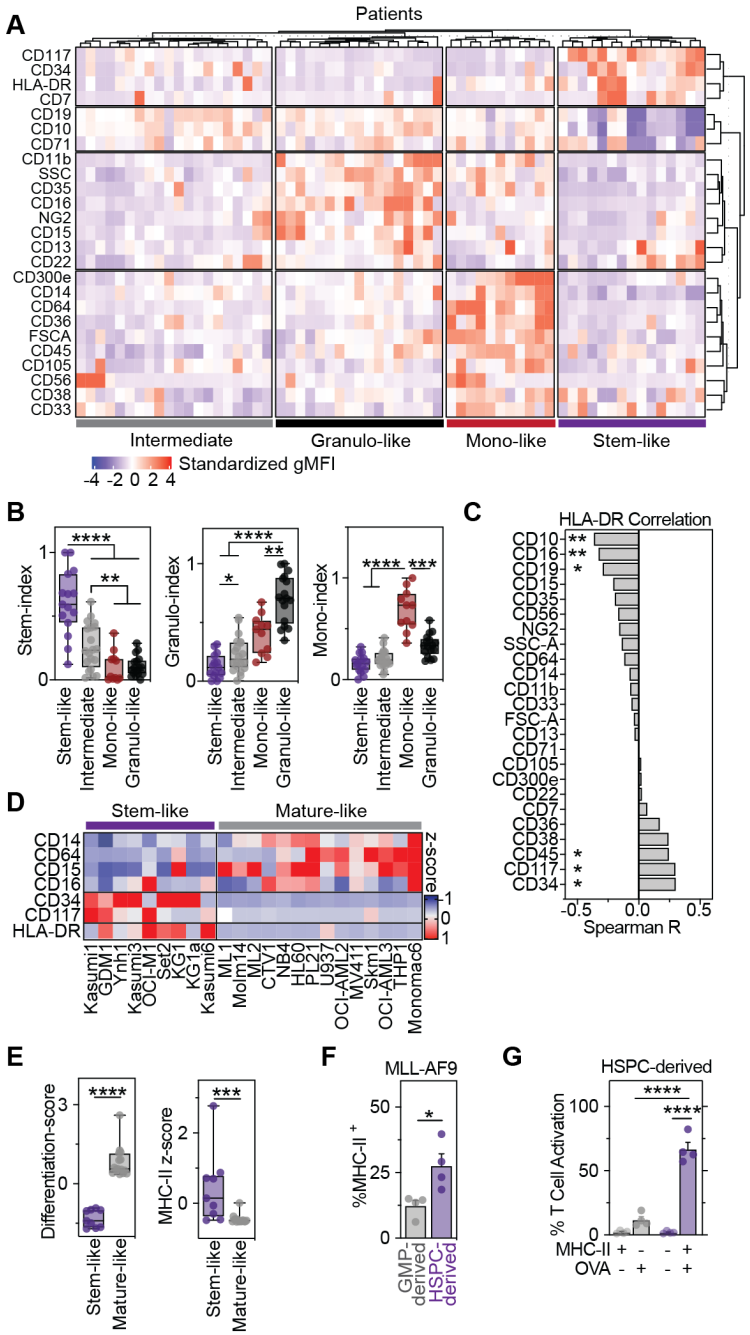

Figure S8. HSPC immunogenic capacities are conserved in stem-like AMLs.

Related to Figure 7.

(**A**) Heatmap showing standardized gMFIs of the EuroFlow flow cytometry markers (van Dongen *et al.*, 2012) across AML patients at diagnosis. Patients and markers were partitioned by PAM clustering. Dendrograms depict within- and between-partition similarities based on hierarchical clustering using Spearman distances, *n=63*.

(**B**) AML patients analyzed with EuroFlow panels were stratified into the indicated groups based on clustering and corresponding indices summarizing expression of stem cell, granulocyte or monocyte marker expression across patient clusters (see Methods).

(**C**) Spearman correlation of HLA-DR expression in the blast compartment of AML patients at diagnosis with other markers measured by the Euroflow panels, *n=63*.

(**D**) AML cell line MHC-II and stemness screen. 23 AML cell lines were characterized based on the depicted markers as stem- or mature-like and HLA-DR surface levels were measured by flow cytometry, *n*=23.
(**E**) Stem-like AML cell lines express higher levels of MHC-II. Differentiation score (left) was calculated as a summed z-score of mature markers from which a summed z-score of stem markers was substracted. HLA-DR (MHC-II) surface expression measured by flow cytometry (right).
(**F**) HSPC-derived AML express higher MHC-II than GMP-derived AML. MLL-AF9 GMP- and LSK-derived AMLs were generated as previously, and MHC-II levels were measured by flow cytometry.
(**G**) HSPC-derived AML T cell activation is MHC-II dependent. MLL-AF9 LSK-derived AMLs were generated as previously, sorted based on MHC-II surface levels and co-cultured with naïve OT-II $CD4^+$ T cells in the presence or absence of OVA. T cell activation is depicted, *n=4*.
Means and SEM are depicted in F and G. No significance = ns, P<0.05 *, P<0.01 **, P<0.001 ***, P<0.0001 ****. Kruskal-Wallis (B) and two-way ANOVA (G) were performed as discovery tests. Spearman correlation coefficients were performed in C. Unpaired Mann-Whitney was test performed in B and E. If not stated otherwise, unpaired two-tailed t-tests were performed as post-hoc tests. In case of multiple comparisons, p-values were corrected according to Benjamini-Hochberg.

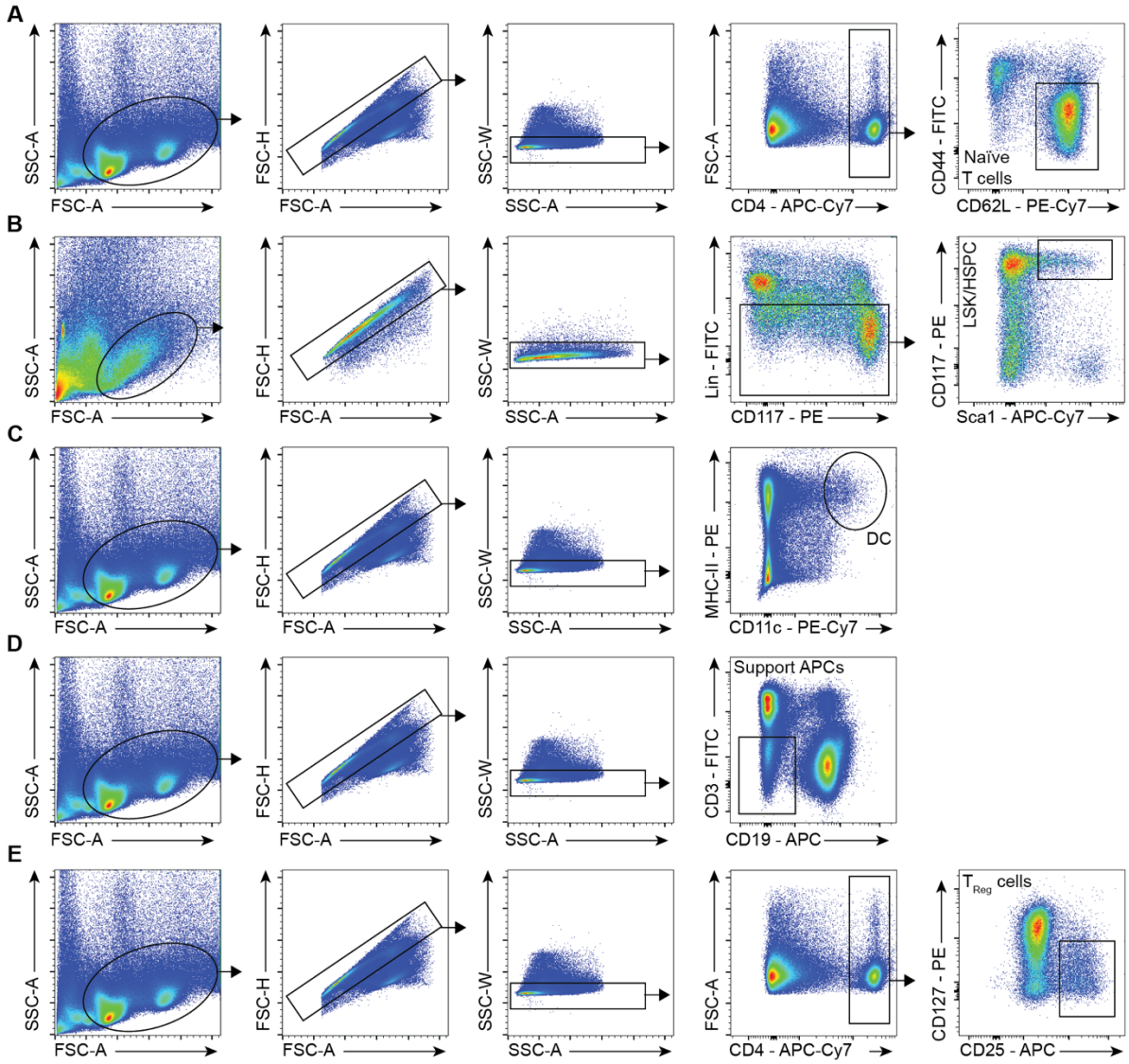

Figure S9. FACS gating strategies I.

(**A**) Naïve $CD4^+$ T cells.

(**B**) HSPCs/LSKs.

(**C**) Dendritic Cells.

(**D**) Splenocytes for *in vitro* suppression assay.

(**E**) Tregs for *in vitro* suppression assay.

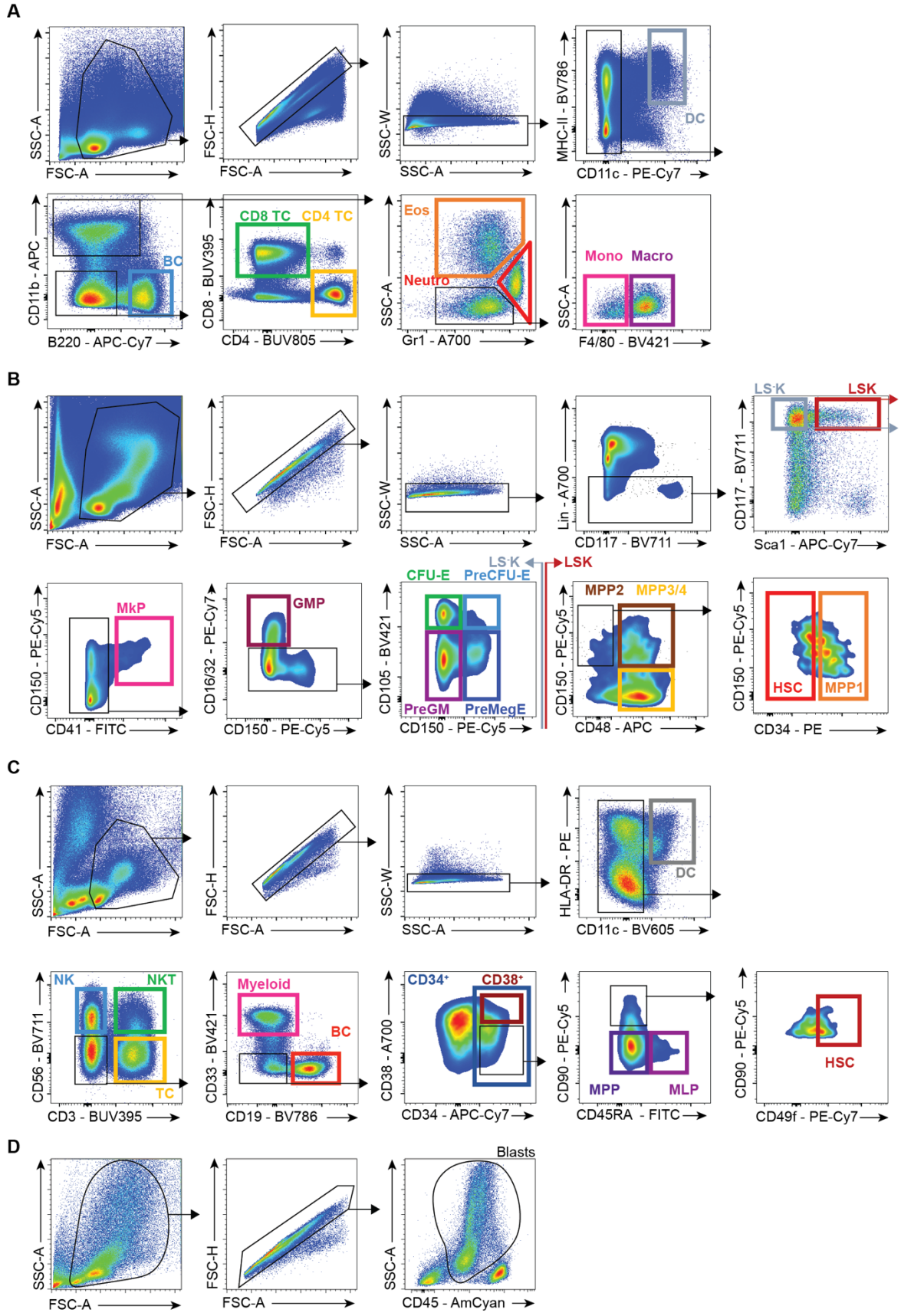

Figure S10. FACS gating strategies II.

(**A**) Mouse mature cell populations gated for different analyses in blood, spleen and bone marrow.

(**B**) Mouse stem and progenitor populations gated for different analyses and sorts.
(**C**) Human mature and stem and progenitor gating strategies for analyses and sorts throughout the study.
(**D**) Gating strategy for human AML blasts cells in the EuroFlow panels.

References

Ali, N. *et al.* (2017) 'Regulatory T Cells in Skin Facilitate Epithelial Stem Cell Differentiation', *Cell*. Elsevier Inc., 169(6), pp. 1119-1129.e11. doi: 10.1016/j.cell.2017.05.002.

Alshetaiwi, H. *et al.* (2020) 'Defining the emergence of myeloid-derived suppressor cells in breast cancer using single-cell transcriptomics', Science Immunology, 5(44), p. eaay6017. doi: 10.1126/sciimmunol.aay6017.

Arpaia, N. *et al.* (2015) 'A Distinct Function of Regulatory T Cells in Tissue Protection', *Cell*. Elsevier Inc., 162(5), pp. 1078–1089. doi: 10.1016/j.cell.2015.08.021.

Baldridge, M. T. *et al.* (2010) 'Quiescent haematopoietic stem cells are activated by IFN-γ in response to chronic infection', *Nature*. Nature Publishing Group, 465(7299), pp. 793–797. doi: 10.1038/nature09135.

Barnden, M. J. *et al.* (1998) 'Defective TCR expression in transgenic mice constructed using cDNA-based α- and β-chain genes under the control of heterologous regulatory elements', *Immunology and Cell Biology*, 76(1), pp. 34–40. doi: 10.1046/j.1440-1711.1998.00709.x.

Barrett, A. J. (2020) 'Acute myeloid leukaemia and the immune system: implications for immunotherapy', *British Journal of Haematology*, 188(1), pp. 147–158. doi: 10.1111/bjh.16310.

Berlin, C. *et al.* (2015) 'Mapping the HLA ligandome landscape of acute myeloid leukemia: a targeted approach toward peptide-based immunotherapy', *Leukemia*, 29(3), pp. 647–659. doi: 10.1038/leu.2014.233.

Bettelli, E. *et al.* (2003) 'Myelin Oligodendrocyte Glycoprotein–specific T Cell Receptor Transgenic Mice Develop Spontaneous Autoimmune Optic Neuritis', *Journal of Experimental Medicine*, 197(9), pp. 1073–1081. doi: 10.1084/jem.20021603.

Biton, M. *et al.* (2018) 'T Helper Cell Cytokines Modulate Intestinal Stem Cell Renewal and Differentiation', *Cell*. Elsevier Inc., 175(5), pp. 1307-1320.e22. doi: 10.1016/j.cell.2018.10.008.

Boettcher, S. and Manz, M. G. (2017) 'Regulation of Inflammation- and Infection-Driven Hematopoiesis', *Trends in Immunology*, 38(5), pp. 345–357. doi: 10.1016/j.it.2017.01.004.

Burzyn, D. *et al.* (2013) 'A Special Population of Regulatory T Cells Potentiates Muscle Repair', *Cell*. Elsevier Inc., 155(6), pp. 1282–1295. doi: 10.1016/j.cell.2013.10.054.

Cabezas-Wallscheid, N. *et al.* (2014) 'Identification of regulatory networks in HSCs and their immediate progeny via integrated proteome, transcriptome, and DNA methylome analysis', *Cell Stem Cell*, 15(4), pp. 507–522. doi: 10.1016/j.stem.2014.07.005.

Charrad, M. *et al.* (2014) 'Nbclust: An R package for determining the relevant number of clusters in a data set', *Journal of Statistical Software*. American Statistical Association, 61(6), pp. 1–36. doi: 10.18637/jss.v061.i06.

Chihara, N. *et al.* (2018) 'Induction and transcriptional regulation of the co-inhibitory gene module in T cells', *Nature*, 558(7710), pp. 454–459. doi: 10.1038/s41586-018-0206-z.

Christopher, M. J. *et al.* (2018) 'Immune Escape of Relapsed AML Cells after Allogeneic Transplantation', *New England Journal of Medicine*, 379(24), pp. 2330–2341. doi: 10.1056/NEJMoa1808777.

Collison, L. W. et al. (2007) 'The inhibitory cytokine IL-35 contributes to regulatory T-cell function', Nature, 450(7169), pp. 566–569. doi: 10.1038/nature06306.

Collison, L. W. et al. (2010) 'IL-35-mediated induction of a potent regulatory T cell population', Nature Immunology. Nature Publishing Group, 11(12), pp. 1093–1101. doi: 10.1038/ni.1952.

Costello, R. *et al.* (1999) 'The immunophenotype of minimally differentiated acute myeloid leukemia (AML-M0): reduced immunogenicity and high frequency of CD34+/CD38−

leukemic progenitors', *Leukemia*, 13(10), pp. 1513–1518. doi: 10.1038/sj.leu.2401519.
Dhaliwal, J. S. *et al.* (2011) 'Susceptibility to aplastic anemia is associated with HLA-DRB1*1501 in an aboriginal population in Sabah, Malaysia', *Human Immunology*. Elsevier Inc., 72(10), pp. 889–892. doi: 10.1016/j.humimm.2011.06.013.
van Dongen, J. J. M. *et al.* (2012) 'EuroFlow antibody panels for standardized n-dimensional flow cytometric immunophenotyping of normal, reactive and malignant leukocytes', *Leukemia*, 26(9), pp. 1908–1975. doi: 10.1038/leu.2012.120.
Doulatov, S. *et al.* (2012) 'Hematopoiesis: A Human Perspective', *Cell Stem Cell*. Elsevier Inc., 10(2), pp. 120–136. doi: 10.1016/j.stem.2012.01.006.
Durbin, J. E. *et al.* (1996) 'Targeted Disruption of the Mouse Stat1 Gene Results in Compromised Innate Immunity to Viral Disease', *Cell*, 84(3), pp. 443–450. doi: 10.1016/S0092-8674(00)81289-1.
Eaves, C. (2015) 'Hematopoietic stem cells: concepts, definitions, and the new reality', *Blood*, 125(17), pp. 2605–2614. doi: 10.1182/blood-2014-12-570200.Lessons.
Essers, M. A. G. *et al.* (2009) 'IFNα activates dormant haematopoietic stem cells in vivo', *Nature*. Nature Publishing Group, 458(7240), pp. 904–908. doi: 10.1038/nature07815.
Falini, B. *et al.* (2019) 'IDH1-R132 changes vary according to NPM1 and other mutations status in AML.', Leukemia, 33(4), pp. 1043–1047. doi: 10.1038/s41375-018-0299-2.
Falk, K. *et al.* (1991) 'Allele-specific motifs revealed by sequencing of self-peptides eluted from MHC molecules', *Nature*, 351(6324), pp. 290–296. doi: 10.1038/351290a0.
Fitchen, J. H., Foon, K. A. and Cline, M. J. (1981) 'The Expression of Histocompatibility-2 Antigens on Hemopoietic Stem Cells', *New England Journal of Medicine*, 305(1). doi: 10.1056/NEJM198107023050104.
Fujisaki, J. *et al.* (2011) 'In vivo imaging of T reg cells providing immune privilege to the haematopoietic stem-cell niche', *Nature*, 474(7350), pp. 216–220. doi: 10.1038/nature10160.
van Galen, P. *et al.* (2014) 'The unfolded protein response governs integrity of the haematopoietic stem-cell pool during stress', *Nature*, 510(7504), pp. 268–272. doi: 10.1038/nature13228.
Genovese, G. *et al.* (2014) 'Clonal Hematopoiesis and Blood-Cancer Risk Inferred from Blood DNA Sequence', *New England Journal of Medicine*, 371(26), pp. 2477–2487. doi: 10.1056/NEJMoa1409405.
Goodnow, C. C. *et al.* (2005) 'Cellular and genetic mechanisms of self tolerance and autoimmunity', *Nature*, 435(7042), pp. 590–597. doi: 10.1038/nature03724.
Gu, Z., Eils, R. and Schlesner, M. (2016) 'Complex heatmaps reveal patterns and correlations in multidimensional genomic data', *Bioinformatics*, 32(18), pp. 2847–2849. doi: 10.1093/bioinformatics/btw313.
Haas, S. *et al.* (2015) 'Inflammation-Induced Emergency Megakaryopoiesis Driven by Hematopoietic Stem Cell-like Megakaryocyte Progenitors', *Cell Stem Cell*, 17(4), pp. 422–434. doi: 10.1016/j.stem.2015.07.007.
Hay, S. B. *et al.* (2018) 'The Human Cell Atlas bone marrow single-cell interactive web portal', *Experimental Hematology*. Elsevier Inc., 68, pp. 51–61. doi: 10.1016/j.exphem.2018.09.004.
Henri, S. *et al.* (2010) 'CD207+ CD103+ dermal dendritic cells cross-present keratinocyte-derived antigens irrespective of the presence of Langerhans cells', *The Journal of Experimental Medicine*, 207(1), pp. 189–206. doi: 10.1084/jem.20091964.
Hirata, Y. *et al.* (2018) 'CD150highBone Marrow Tregs Maintain Hematopoietic Stem Cell

Quiescence and Immune Privilege via Adenosine', *Cell Stem Cell*. Elsevier Inc., 22(3), pp. 445-453.e5. doi: 10.1016/j.stem.2018.01.017.
Hirche, C. *et al.* (2017) 'Systemic Virus Infections Differentially Modulate Cell Cycle State and Functionality of Long-Term Hematopoietic Stem Cells In Vivo', *Cell Reports*, 19(11), pp. 2345–2356. doi: 10.1016/j.celrep.2017.05.063.
Ho, T. T. *et al.* (2017) 'Autophagy maintains the metabolism and function of young and old stem cells', *Nature*, 543(7644), pp. 205–210. doi: 10.1038/nature21388.
Jaiswal, S. *et al.* (2014) 'Age-related clonal hematopoiesis associated with adverse outcomes.', *The New England journal of medicine*, 371(26), pp. 2488–98. doi: 10.1056/NEJMoa1408617.
Jakubzick, C. V., Randolph, G. J. and Henson, P. M. (2017) 'Monocyte differentiation and antigen-presenting functions', *Nature Reviews Immunology*. Nature Publishing Group, 17(6), pp. 349–362. doi: 10.1038/nri.2017.28.
Jurewicz, M. M. and Stern, L. J. (2019) 'Class II MHC antigen processing in immune tolerance and inflammation', *Immunogenetics*. Immunogenetics, 71(3), pp. 171–187. doi: 10.1007/s00251-018-1095-x.
Käll, L. *et al.* (2007) 'Semi-supervised learning for peptide identification from shotgun proteomics datasets', *Nature Methods*, 4(11), pp. 923–925. doi: 10.1038/nmeth1113.
Kambayashi, T. and Laufer, T. M. (2014) 'Atypical MHC class II-expressing antigen-presenting cells: can anything replace a dendritic cell?', *Nature Reviews Immunology*, 14(11), pp. 719–730. doi: 10.1038/nri3754.
King, K. Y. and Goodell, M. A. (2011) 'Inflammatory modulation of HSCs: viewing the HSC as a foundation for the immune response', *Nature Reviews Immunology*. Nature Publishing Group, 11(10), pp. 685–692. doi: 10.1038/nri3062.
Klimmeck, D. *et al.* (2014) 'Transcriptome-wide Profiling and Posttranscriptional Analysis of Hematopoietic Stem/Progenitor Cell Differentiation toward Myeloid Commitment', *Stem Cell Reports*. The Authors, 3(5), pp. 858–875. doi: 10.1016/j.stemcr.2014.08.012.
Kohlmann, A. *et al.* (2010) 'Gene expression profiling in AML with normal karyotype can predict mutations for molecular markers and allows novel insights into perturbed biological pathways', *Leukemia*, 24(6), pp. 1216–1220. doi: 10.1038/leu.2010.73.
Kowalewski, D. J. and Stevanović, S. (2013) 'Biochemical Large-Scale Identification of MHC Class I Ligands', in *Methods Mol Biol*, pp. 145–157. doi: 10.1007/978-1-62703-218-6_12.
Krivtsov, A. V *et al.* (2006) 'Transformation from committed progenitor to leukaemia stem cell initiated by MLL-AF9', *Nature*, 442(7104), pp. 818–822. doi: 10.1038/nature04980.
Krivtsov, A. V *et al.* (2013) 'Cell of origin determines clinically relevant subtypes of MLL-rearranged AML.', *Leukemia*, 27(4), pp. 852–60. doi: 10.1038/leu.2012.363.
Ley, T. J. *et al.* (2013) 'Genomic and Epigenomic Landscapes of Adult De Novo Acute Myeloid Leukemia', *New England Journal of Medicine*, 368(22), pp. 2059–2074. doi: 10.1056/NEJMoa1301689.
Liao, D. *et al.* (2019) 'A review of efficacy and safety of checkpoint inhibitor for the treatment of acute myeloid leukemia', *Frontiers in Pharmacology*, 10(JUN), pp. 1–11. doi: 10.3389/fphar.2019.00609.
Liu, S. *et al.* (2016) 'Association of Human Leukocyte Antigen DRB1*15 and DRB1*15:01 Polymorphisms with Response to Immunosuppressive Therapy in Patients with Aplastic Anemia: A Meta-Analysis', *PLOS ONE*. Edited by J. Devaney, 11(9), p. e0162382. doi: 10.1371/journal.pone.0162382.
Love, M. I., Huber, W. and Anders, S. (2014) 'Moderated estimation of fold change and

dispersion for RNA-seq data with DESeq2', *Genome Biology*, 15(12), p. 550. doi: 10.1186/s13059-014-0550-8.
Maechler, M. *et al.* (2019) 'cluster: Cluster Analysis Basics and Extensions. R package version 2.1.0.'
Matatall, K. A. *et al.* (2014) 'Type II Interferon Promotes Differentiation of Myeloid-Biased Hematopoietic Stem Cells', *STEM CELLS*, 32(11), pp. 3023–3030. doi: 10.1002/stem.1799.
Merad, M., Sathe, P., Helft, J., Miller, J. & Mortha, A. The Dendritic Cell Lineage: Ontogeny and Function of Dendritic Cells and Their Subsets in the Steady State and the Inflamed Setting. Annu. Re', *Annual Review of Immunology*, 31(1), pp. 563–604. doi: 10.1146/annurev-immunol-020711-074950.
Miale, T. D. *et al.* (1982) 'Surface la-Like Expression and MLR-Stimulating Capacity of Human Leukemic Myeloblasts: Implications for Immunotherapy and Prognosis', *Acta Haematologica*, 68(1), pp. 3–13. doi: 10.1159/000206941.
Murphy, D. B. *et al.* (1989) 'A novel MHC class II epitope expressed in thymic medulla but not cortex', *Nature*, 338(6218), pp. 765–768. doi: 10.1038/338765a0.
Mutis, T. *et al.* (1997) 'HLA Class II Restricted T-Cell Reactivity to a Developmentally Regulated Antigen Shared by Leukemic Cells and CD34+ Early Progenitor Cells', *Blood*, 90(3), pp. 1083–1090. doi: 10.1182/blood.V90.3.1083.1083_1083_1090.
Mutis, T. *et al.* (1998) 'CD80-Transfected Acute Myeloid Leukemia Cells Induce Primary Allogeneic T-Cell Responses Directed at Patient Specific Minor Histocompatibility Antigens and Leukemia-Associated Antigens', *Blood*, 92(5), pp. 1677–1684. doi: 10.1182/blood.V92.5.1677.417k14_1677_1684.
Naik, S. *et al.* (2018) 'Two to Tango: Dialog between Immunity and Stem Cells in Health and Disease', *Cell*. Elsevier Inc., 175(4), pp. 908–920. doi: 10.1016/j.cell.2018.08.071.
Nakao, S. *et al.* (1994) 'Identification of a specific HLA class II haplotype strongly associated with susceptibility to cyclosporine-dependent aplastic anemia', *Blood*, 84(12), pp. 4257–4261. doi: 10.1182/blood.V84.12.4257.bloodjournal84124257.
Neefjes, J. *et al.* (2011) 'Towards a systems understanding of MHC class I and MHC class II antigen presentation', *Nature Reviews Immunology*. Nature Publishing Group, 11(12), pp. 823–836. doi: 10.1038/nri3084.
Ness, S., Lin, S. and Gordon, J. R. (2021) 'Regulatory Dendritic Cells, T Cell Tolerance, and Dendritic Cell Therapy for Immunologic Disease', *Frontiers in Immunology*, 12. doi: 10.3389/fimmu.2021.633436.
Newman, R. A. *et al.* (1983) 'Differential expression of HLA-DR and DR-linked determinants on human leukemias and lymphoid cells', *European Journal of Immunology*, 13(2), pp. 172–176. doi: 10.1002/eji.1830130215.
Ng, S. W. K. *et al.* (2016) 'A 17-gene stemness score for rapid determination of risk in acute leukaemia', *Nature*. Nature Publishing Group, 540(7633), pp. 433–437. doi: 10.1038/nature20598.
Nimer, S. D. *et al.* (1994) 'An increased HLA DR2 frequency is seen in aplastic anemia patients.', *Blood*, 84(3), pp. 923–7.
Novershtern, N. *et al.* (2011) 'Densely Interconnected Transcriptional Circuits Control Cell States in Human Hematopoiesis', *Cell*. Elsevier Inc., 144(2), pp. 296–309. doi: 10.1016/j.cell.2011.01.004.
Pellin, D. *et al.* (2019) 'A comprehensive single cell transcriptional landscape of human hematopoietic progenitors', *Nature Communications*, 10(1), p. 2395. doi: 10.1038/s41467-019-10291-0.

Picelli, S. *et al.* (2013) 'Smart-seq2 for sensitive full-length transcriptome profiling in single cells', Nature Methods, 10(11), pp. 1096–1098. doi: 10.1038/nmeth.2639.
Picelli, S. *et al.* (2014) 'Full-length RNA-seq from single cells using Smart-seq2', Nature Protocols, 9(1), pp. 171–181. doi: 10.1038/nprot.2014.006.
Pierini, A. *et al.* (2017) 'Foxp3+ regulatory T cells maintain the bone marrow microenvironment for B cell lymphopoiesis', *Nature Communications*. Nature Publishing Group, 8(1), p. 15068. doi: 10.1038/ncomms15068.
Pietras, E. M. *et al.* (2016) 'Chronic interleukin-1 exposure drives haematopoietic stem cells towards precocious myeloid differentiation at the expense of self-renewal', *Nature Cell Biology*, 18(6), pp. 607–618. doi: 10.1038/ncb3346.
Pietras, E. M. (2017) 'Inflammation: a key regulator of hematopoietic stem cell fate in health and disease', *Blood*, 130(15), pp. 1693–1698. doi: 10.1182/blood-2017-06-780882.
Pölönen, P. *et al.* (2019) 'Hemap: An Interactive Online Resource for Characterizing Molecular Phenotypes across Hematologic Malignancies', Cancer Research, 79(10), pp. 2466–2479. doi: 10.1158/0008-5472.CAN-18-2970.
Rehman, S. *et al.* (2009) 'The Frequency of HLA Class I and II Alleles in Pakistani Patients with Aplastic Anemia', *Immunological Investigations*, 38(8), pp. 812–819. doi: 10.3109/08820130903271415.
Roche, P. A. and Furuta, K. (2015) 'The ins and outs of MHC class II-mediated antigen processing and presentation', *Nature Reviews Immunology*. Nature Publishing Group, 15(4), pp. 203–216. doi: 10.1038/nri3818.
Rudensky, A. Y. *et al.* (1991) 'On the complexity of self', *Nature*, 353(6345), pp. 660–662. doi: 10.1038/353660a0.
Russell, J. L. and Engh, G. J. (1979) 'The Expression of Histocompatibility-2 Antigens on Hemopoietic Stem Cells', *Tissue Antigens*, 13. doi: http://doi.wiley.com/10.1111/j.1399-0039.1979.tb01135.x.
Sato, T. *et al.* (2009) 'Interferon regulatory factor-2 protects quiescent hematopoietic stem cells from type I interferon–dependent exhaustion', *Nature Medicine*, 15(6), pp. 696–700. doi: 10.1038/nm.1973.
Sauntharajah, Y. *et al.* (2002) 'HLA-DR15 (DR2) is overrepresented in myelodysplastic syndrome and aplastic anemia and predicts a response to immunosuppression in myelodysplastic syndrome', *Blood*, 100(5), pp. 1570–1574. doi: 10.1182/blood.V100.5.1570.h81702001570_1570_1574.
Schumacher, T. *et al.* (2014) 'A vaccine targeting mutant IDH1 induces antitumour immunity', *Nature*, 512(7514), pp. 324–327. doi: 10.1038/nature13387.
Spencer, S. D. *et al.* (1998) 'The Orphan Receptor CRF2-4 Is an Essential Subunit of the Interleukin 10 Receptor', Journal of Experimental Medicine, 187(4), pp. 571–578. doi: 10.1084/jem.187.4.571.
Sieff, C. *et al.* (1982) 'Changes in Cell Surface Antigen Expression During Hemopoietic Differentiation', *Blood*, 60(3).
Steimle, V. *et al.* (1993) 'Complementation cloning of an MHC class II transactivator mutated in hereditary MHC class II deficiency (or bare lymphocyte syndrome)', *Cell*, 75(1), pp. 135–146. doi: 10.1016/S0092-8674(05)80090-X.
Steimle, V. *et al.* (1994) 'Regulation of MHC class II expression by interferon-γ mediated by the transactivator gene CIITA', *Science*, 265(5168), pp. 106–109. doi: 10.1126/science.8016643.
Steinman, R. M. (2007) 'Dendritic cells: Understanding immunogenicity', *European Journal*

of Immunology, 37(SUPPL. 1), pp. 53–60. doi: 10.1002/eji.200737400.
Szer, J. *et al.* (1985) 'Failure of autologous marrow reconstitution after cytolytic treatment of marrow with anti-Ia monoclonal antibody', *Blood*, 65(4), pp. 819–822. doi: 10.1182/blood.v65.4.819.bloodjournal654819.
Takizawa, H. *et al.* (2017) 'Pathogen-Induced TLR4-TRIF Innate Immune Signaling in Hematopoietic Stem Cells Promotes Proliferation but Reduces Competitive Fitness', *Cell Stem Cell*, 21(2), pp. 225-240.e5. doi: 10.1016/j.stem.2017.06.013.
Toffalori, C. *et al.* (2019) 'Immune signature drives leukemia escape and relapse after hematopoietic cell transplantation', *Nature Medicine*. Springer US, 25(4), pp. 603–611. doi: 10.1038/s41591-019-0400-z.
Urbieta, M. *et al.* (2010) 'Hematopoietic progenitor cell regulation by CD4+CD25+ T cells', *Blood*, 115(23), pp. 4934–4943. doi: 10.1182/blood-2009-04-218826.
Vago, L. and Gojo, I. (2020) 'Immune escape and immunotherapy of acute myeloid leukemia', *Journal of Clinical Investigation*, 130(4), pp. 1552–1564. doi: 10.1172/JCI129204.
Wakkach, A. *et al.* (2003) 'Characterization of Dendritic Cells that Induce Tolerance and T Regulatory 1 Cell Differentiation In Vivo', *Immunity*, 18(5), pp. 605–617. doi: 10.1016/S1074-7613(03)00113-4.
Walter, D. *et al.* (2015) 'Exit from dormancy provokes DNA-damage-induced attrition in haematopoietic stem cells', *Nature*, 520(7548), pp. 549–552. doi: 10.1038/nature14131.
Young, N. S. (2018) 'Aplastic Anemia', *New England Journal of Medicine*, 379(17), pp. 1643–1656. doi: 10.1056/NEJMra1413485.
Yu, G. *et al.* (2012) 'clusterProfiler: an R Package for Comparing Biological Themes Among Gene Clusters', *OMICS: A Journal of Integrative Biology*, 16(5), pp. 284–287. doi: 10.1089/omi.2011.0118.
Zhang, H. *et al.* (2016) 'Sepsis Induces Hematopoietic Stem Cell Exhaustion and Myelosuppression through Distinct Contributions of TRIF and MYD88', *Stem Cell Reports*, 6(6), pp. 940–956. doi: 10.1016/j.stemcr.2016.05.002.
Zhang, H. *et al.* (2020) 'An IL-27-Driven Transcriptional Network Identifies Regulators of IL-10 Expression across T Helper Cell Subsets', Cell Reports, 33(8), p. 108433. doi: 10.1016/j.celrep.2020.108433.
Zhu, J. and Paul, W. E. (2010) 'Peripheral CD4+ T-cell differentiation regulated by networks of cytokines and transcription factors', Immunological Reviews, 238(1), pp. 247–262. doi: 10.1111/j.1600-065X.2010.00951.x.
Zou, L. *et al.* (2004) 'Bone Marrow Is a Reservoir for CD4 + CD25 + Regulatory T Cells that Traffic through CXCL12/CXCR4 Signals', *Cancer Research*, 64(22), pp. 8451–8455. doi: 10.1158/0008-5472.CAN-04-1987.